

1 **Investigation of the summer 2018 European ozone air pollution episodes using**  
2 **novel satellite data and modelling**

3 Richard J. Pope<sup>1,2</sup>, Brian J. Kerridge<sup>3,4</sup>, Martyn P. Chipperfield<sup>1,2</sup>, Richard Siddans<sup>3,4</sup>, Barry G. Latter<sup>3,4</sup>,  
4 Lucy J. Ventress<sup>3,4</sup>, Matilda A. Pimlott<sup>1</sup>, Wuhu Feng<sup>1,5</sup>, Edward Comyn-Platt<sup>6</sup>, Garry D. Hayman<sup>7</sup>,  
5 Stephen R. Arnold<sup>1</sup> and Ailish M. Graham<sup>1</sup>

6  
7 *1: School of Earth and Environment, University of Leeds, Leeds, United Kingdom*

8  
9 *2: National Centre for Earth Observation, University of Leeds, Leeds, United Kingdom*

10  
11 *3: Remote Sensing Group, STFC Rutherford Appleton Laboratory, Chilton, United Kingdom*

12  
13 *4: National Centre for Earth Observation, STFC Rutherford Appleton Laboratory, Chilton, United*  
14 *Kingdom*

15  
16 *5: National Centre for Atmospheric Science, University of Leeds, Leeds, United Kingdom*

17  
18 *6: European Centre for Medium-Range Weather Forecasts, Reading, UK*

19  
20 *7: Centre for Ecology and Hydrology, Wallingford, United Kingdom*  
21

22 Submitted to *Atmospheric Chemistry and Physics*

23 Correspondence to: Richard J. Pope (r.j.pope@leeds.ac.uk)

24 **Abstract:**

25 In the summer of 2018, Europe experienced an intense heat wave which coincided with several  
26 persistent large-scale ozone (O<sub>3</sub>) pollution episodes. Novel satellite data of lower tropospheric  
27 column O<sub>3</sub> from the Global Ozone Monitoring Experiment-2 (GOME-2) and Infrared Atmospheric  
28 Sounding Interferometer (IASI) on the MetOp satellite showed substantial enhancements in 2018  
29 relative to other years since 2012. Surface observations also showed ozone enhancements across  
30 large regions of continental Europe in summer 2018 compared to 2017. Enhancements to surface  
31 temperature and the O<sub>3</sub> precursor gases carbon monoxide and methanol in 2018 were co-retrieved  
32 from MetOp observations by the same scheme. This analysis was supported by the TOMCAT  
33 chemistry transport model (CTM) to investigate processes driving the observed O<sub>3</sub> enhancements.  
34 Through several targeted sensitivity experiments we show that meteorological processes, and  
35 emissions to a secondary order, were important for controlling the elevated O<sub>3</sub> concentrations at the  
36 surface. However, mid-tropospheric (~500 hPa) O<sub>3</sub> enhancements were dominated by  
37 meteorological processes. We find that contributions from stratospheric O<sub>3</sub> intrusions ranged  
38 between 15 - 40%. Analysis of back trajectories indicates that the import of O<sub>3</sub>-enriched air masses  
39 into Europe originated over the North Atlantic substantially increasing O<sub>3</sub> in the 500 hPa layer during  
40 summer 2018.

43 **1. Introduction**

44 Over the past two decades there have been several intense summer-time heatwaves over Europe  
45 (e.g. 2003 over continental Europe (Scott et al., 2004), 2006 over north-western Europe (Rebetz et  
46 al., 2008) and 2010 across eastern Europe and Russia (Matsueda et al., 2011)). With current and  
47 future climate change, increasing average global surface temperature is expected to trigger more  
48 frequent and intense heatwaves (Lhotka et al., 2017; Guerreiro et al., 2018). The summer-time 2018  
49 heatwave across predominantly north-western and central Europe and Scandinavia generated  
50 temperature anomalies of approximately 2.0-4.0 K (Li et al., 2020; Drouard et al., 2020). Dynamically,  
51 it was caused by a combination of intense anticyclonic blocking systems, Rossby wave dynamics and  
52 the positive phase of the summer-time North Atlantic Oscillation (NAO+) (Li et al., 2020; Liu et al.,  
53 2020; Drouard et al., 2020). Environmentally, the summer 2018 heatwave caused severe drought  
54 conditions with decreased precipitation and soil moisture content (Bastos et al., 2020; Dirmeyer et  
55 al., 2020), while negatively impacting natural vegetation (e.g. decreased gross primary productivity  
56 (Smith et al., 2020; Bastos et al., 2020)). From a human health perspective, the 2018 heatwave  
57 caused 863 temperature related excess deaths in the UK (PHE, 2019).

58 As well as meteorological and vegetation responses, enhancements in atmospheric pollutants from  
59 heatwaves can lead to a degradation in air quality (AQ) across Europe. Blocking systems (anticyclonic  
60 conditions) have been shown to increase the level of air pollutions such as carbon monoxide (CO;  
61 Thomas and Devasthale, 2014), nitrogen dioxide (NO<sub>2</sub>; Pope et al., 2014) and particulate matter (i.e.  
62 PM<sub>2.5</sub>; Graham et al., 2020) to hazardous levels. Pope et al., (2016) focused on the 2006 UK  
63 heatwave and detected enhancements in surface O<sub>3</sub> through the accumulation of pollutants (i.e.  
64 atmospheric blocking) but also the higher temperatures yielding more active atmospheric chemistry  
65 (i.e. ozone formation). Papanastasiou et al., (2015) found that Greek heatwave conditions (2001-  
66 2010) typically yielded an increase in NO<sub>2</sub>, PM<sub>2.5</sub> and O<sub>3</sub> by 14-29%, 25-38% and 12%, respectively.  
67 Rasilla et al., (2019) found that heatwaves in Madrid only moderately increased NO<sub>2</sub> and O<sub>3</sub> but  
68 significantly increased PM<sub>10</sub> concentrations. However, they associated this with enhanced long-  
69 range transport of African dust and then accumulation under heatwave conditions. García-Herrera et  
70 al., (2010) provided a review of the 2003 European heatwave finding that the Alpine region had  
71 substantially elevated surface ozone levels (peaking at 417 µg/m<sup>3</sup> with 68% of sites from 23  
72 countries reaching concentrations above 180 µg/m<sup>3</sup>) when compared with the previous 12 summers.  
73 Biogenic volatile organic compound (BVOC) emissions from vegetation are known to increase under  
74 drought conditions from temperature stress (e.g. in the 2003 European heatwave; Rennenberg et  
75 al., 2006). Churkina et al., (2017) found that heatwave conditions (2006) in Berlin yielded an increase  
76 in BVOC emissions which contributed up to 12% of the surface ozone formation. Heatwaves can also  
77 trigger wildfires, which emit primary air pollutions and can form secondary gases such as surface  
78 ozone on a regional and hemispheric scale (Honrath et al., 2004). Overall, elevated surface O<sub>3</sub> is  
79 associated with adverse health impacts (Doherty et al., 2017; Heal et al., 2013; Jerrett et al., 2009)  
80 with ailments such as asthma, reduced lung function and disease (WHO, 2021). It also has adverse  
81 impacts on the natural biosphere (Sitch et al., 2007) and agriculture (Hollaway et al., 2012; van  
82 Dingenen et al., 2009), in turn reducing deposition of surface ozone on vegetation. In this study, we  
83 use surface and satellite observations of O<sub>3</sub>, in combination with the well-evaluated TOMCAT global  
84 chemical transport model (CTM), to investigate the impact of the summer 2018 heatwave on  
85 European AQ and determine the key processes driving observed surface/tropospheric O<sub>3</sub>

86 enhancements. We describe the observations and model we have used in Section 2. Section 3 and  
87 Section 4 discusses our results and discussion/conclusions, respectively.

## 88 **2. Observations and Model**

### 89 **2.1. Satellite and Surface Observations**

90 We use satellite observations of lower tropospheric O<sub>3</sub> (i.e. sub-column O<sub>3</sub> (SCO<sub>3</sub>) between the  
91 surface and 450 hPa) from the Global Ozone Monitoring Experiment (GOME-2) and the Infrared  
92 Atmospheric Sounding Interferometer (IASI) instruments on-board ESA's MetOp-A satellite, which  
93 was launched in 2006 into a sun-synchronous polar orbit with equator crossing times of 9:30 (day)  
94 and 21:30 (night). GOME-2 is a nadir-viewing spectrometer with spectral coverage in the ultraviolet-  
95 visible (UV-Vis) of 240–790 nm (Riese et al., 2012) and a ground footprint of 40 km × 80 km in the  
96 first part of the mission and 40 km x 40 km from 2013 (once Metop-B was commissioned). IASI is a  
97 Michelson interferometer which observes the infrared spectral range 645 to 2760 cm<sup>-1</sup> with spectral  
98 sampling of 0.25 cm<sup>-1</sup> (Illingworth et al., 2011). It measures simultaneously in four fields of view  
99 (circular at nadir with a diameter of 12 km) which are scanned across track to sample a 2200 km-  
100 wide swath (Clerbaux et al., 2009).

101 For GOME-2, the Rutherford Appleton Laboratory (RAL) scheme uses an optimal estimation  
102 algorithm (Rodgers, 2000) to retrieve height-resolved ozone distributions spanning the stratosphere  
103 and troposphere (Miles et al., 2015). The scheme applied to GOME-2 has been developed from that  
104 used first for GOME-1 on-board ERS-2 (Munro et al., 1998; Forster et al., 2007). This is a multi-step  
105 scheme in which profile information is first retrieved in the stratosphere by exploiting wavelength-  
106 dependent absorption in the O<sub>3</sub> Hartley band (270-307nm) and is then extended into the  
107 troposphere by exploiting temperature-dependent spectral structure in the O<sub>3</sub> Huggins bands (325-  
108 335nm). For IASI, O<sub>3</sub> profiles are retrieved using an extended version of RAL's Infrared-Microwave-  
109 Sounding (IMS) scheme, which is described in Pope et al., (2021), Palmer et al., (2022) and Pimlott et  
110 al., (2022). The IMS core scheme was originally developed to retrieve temperature, water vapour  
111 and stratospheric O<sub>3</sub> profiles along with surface spectral emissivity and cloud jointly from co-located  
112 measurements by IASI, the Microwave Humidity Sounder (MHS) and the Advanced Microwave  
113 Sounding Unit (AMSU-A) on MetOp (RAL Space, 2015). GOME-2 and IMS O<sub>3</sub> data were filtered for a  
114 geometric cloud fraction less than 0.2, a solar zenith angle less than 80°, a cost function less than  
115 200.0 and a convergence flag equal to 1.0. Examples of the vertical sensitivity to retrieving ozone  
116 (i.e. averaging kernels) from GOME-2 and IMS are shown in **Supplementary Material (SM) 1**.

117 We also use surface O<sub>3</sub> observations from the European Monitoring and Evaluation Programme  
118 (EMEP) network for May-August 2017 and 2018. The EMEP network contains >100 surface  
119 measurement sites measuring information on a range of air pollutions (e.g. ozone, NO<sub>2</sub> and PM<sub>2.5</sub>).  
120 EMEP surface data can be used for multiple scientific applications such as trends analysis (Yan et al.,  
121 2018) and atmospheric chemistry model evaluation (Schultz et al., 2017; Archibald et al., 2020) and  
122 is hosted by the EBAS database infrastructure, developed by the Norwegian Institute for Air  
123 Research. In total, we used 125 spatial collocated EMEP sites in both years across Europe. Here, data  
124 at individual sites were selected where the corresponding data flag was set to 0.0.

### 125 **2.2. Modelling & Sensitivity Experiments**

126 In this study the TOMCAT CTM (Chipperfield, 2006) is forced by European Centre for Medium-Range  
127 Weather Forecasts (ECMWF) ERA-Interim reanalysis meteorology (Dee et al., 2011) and is run at a

128 horizontal resolution of  $2.8^\circ \times 2.8^\circ$ . The model has with 31 vertical levels from the surface to 10 hPa  
129 with 5-7 (approximately 10) levels in the boundary layer (mid-troposphere), depending on latitude.  
130 The model includes detailed tropospheric chemistry, including 229 gas-phase reactions and 82  
131 advected tracers (Monks et al., 2017), and heterogeneous chemistry driven by size-resolved aerosol  
132 from the GLOMAP module (Mann et al., 2010). Anthropogenic emissions used in this study come  
133 from MACCity (Granier et al., 2011). The original dataset in Granier et al., (2011) derived emissions  
134 up to 2010. Therefore, the Representative Concentration Pathways 8.5 (RCP 8.5) were used by  
135 Granier et al., (2011) to generate emissions for later years (e.g. 2017 and 2018 as used in this study).  
136 Fire emissions are from the Global Fire Assimilation System (GFAS, Kaiser et al., 2012) for 2017 and  
137 2018. Year-specific off-line biogenic volatile organic compounds (VOCs) emissions for acetone,  
138 methanol, isoprene and monoterpenes were simulated by the Joint UK Land Environment Simulator  
139 (JULES – Pacifico et al., 2011; Best et al., 2011; Clark et al., 2011). All other biogenic VOC emissions  
140 are climatological values and provided by the Chemistry-Climate Model Initiative (CCMI)  
141 (Morgenstern et al., 2017). The global budgets of the JULES VOC emissions are low in comparison to  
142 the climatological CCMI emissions, so were scaled up on a regional basis, while retaining the 2017-  
143 2018 step change related to the 2018 summer heat wave. The full details of JULES VOC emissions  
144 scaling can be found in **SM4**. Lightning emissions of  $\text{NO}_x$  are coupled to convection in the model,  
145 which is derived from the meteorological reanalyses. Therefore, they vary in space and time  
146 according to the seasonality and spatial pattern of convective activity (Stockwell et al., 1999). The  
147 model was run for 2017 and 2018 with output at 6-hourly intervals (i.e. 00, 06, 12 and 18 UTC). Here,  
148 each year was run with its respective meteorology and emissions and given the labels  
149 Met17\_Emis17 (representing 2017) and Met18\_Emis18 (representing 2018).

150 To explore the importance of emission and meteorological processes behind the elevated European  
151 summer 2018 tropospheric  $\text{O}_3$  levels, a 1-year model sensitivity experiment was performed using  
152 2018 meteorology but 2017 emissions (i.e. Met18\_Emis17). Therefore, the difference between  
153 Met18\_Emis17 and Met17\_Emis17 highlights the impact of fixed emissions (i.e. 2017 emissions for  
154 both years), while the Met18\_Emis18 minus Met18\_Emis17 highlights the impact of fixed  
155 meteorology (i.e. 2018 meteorology for both years – including BVOC emissions). These are  
156 compared with the control differences for 2018-2017 (Met18\_Emis18- Met17\_Emis17). From here  
157 on in, we refer to the control differences, fixed emission differences and the fixed meteorology  
158 differences as CTL\_DIFF, FIXED\_EMIS\_DIFF and FIXED\_MET\_DIFF, respectively. TOMCAT also  
159 includes a stratospheric  $\text{O}_3$  tracer, a common approach to tag stratospheric  $\text{O}_3$  (e.g. Roelofs et al.,  
160 2003; Akritidis et al., 2019), which can be used to investigate the impact of stratospheric  $\text{O}_3$  intrusion  
161 into the troposphere. The tracer is set equal to the model-calculated  $\text{O}_3$  in the stratosphere. The only  
162 tropospheric source of  $\text{O}_{35}$  is transport from the stratosphere while its sinks are via photolysis,  
163 reactions with  $\text{HO}_2$ , OH and  $\text{H}_2\text{O}$  through  $\text{O}(^1\text{D})$  produced from  $\text{O}_{35}$  and surface deposition (Monks et  
164 al., 2017). The tracer does not have a fixed lifetime but the loss rate in the troposphere depends on  
165 the modelled local OH,  $\text{HO}_2$ ,  $\text{H}_2\text{O}$  and photolysis. Any  $\text{O}_3$  that gets into the stratosphere will be  
166 labelled as stratospheric before it returns. This was used to investigate the impact of stratospheric  
167  $\text{O}_3$  intrusion into the troposphere.

168 TOMCAT has been used in a number of previous studies to investigate air quality and tropospheric  
169 composition (e.g. Richards et al., 2013; Emmons et al., 2015; Pope et al., 2018; Pope et al., 2020)  
170 whose results give confidence in the model's ability to simulate European tropospheric  $\text{O}_3$  in this  
171 study. Overall, when compared with observations, TOMCAT has good spatial agreement with both

172 GOME-2 and IASI and can reasonably reproduce the 2018 SCO<sub>3</sub> enhancement in 2018 versus 2017  
173 (**SM 5**). The model also has good agreement, both in magnitude and seasonality, with the EMEP  
174 observed surface concentrations (**SM 5**). TOMCAT surface ozone was also compared with higher  
175 resolution modelling (reanalysis) data from the Copernicus Atmosphere Monitoring Service (CAMS),  
176 which showed good spatial agreement between the modelling data sets and in the simulated surface  
177 ozone absolute values during the European summer 2018 pollution episode (**SM 5**).

### 178 **2.3 ROTRAJ Back-trajectories**

179 We use the Reading Offline Trajectory Model (ROTRAJ) to generate air mass back-trajectories  
180 (Methven et al., 2003) to assess the import of tropospheric O<sub>3</sub> into Europe. ROTRAJ is a Lagrangian  
181 atmospheric transport model driven by meteorology from the same ECMWF ERA-Interim reanalyses  
182 (horizontal resolution of 1.0125°) as used by TOMCAT. Velocity fields at the Lagrangian particle  
183 positions are determined by cubic Lagrange interpolation in the vertical, bilinear interpolation in the  
184 horizontal and linear interpolation in time. This method accounts for large scale advection since the  
185 winds are resolved but does not resolve small scale sub-grid turbulent transport. Kinematic back-  
186 trajectories were released at 6-hourly intervals (i.e. at 00, 06, 12 and 18 UTC) from Paris and Berlin,  
187 both central locations over Europe in the region of summer-time 2018 O<sub>3</sub> enhancements, between  
188 the 1<sup>st</sup> May and 31<sup>st</sup> August for both 2017 and 2018. The trajectories were released at the surface  
189 and at approximately 500 hPa and integrated for 10 days with 6-hourly output (i.e. 41 trajectory  
190 points including the starting location) to investigate the origin of air masses arriving in these altitude  
191 regions of enhanced summer-time O<sub>3</sub> in 2018. In total, ROTRAJ was therefore run 8 times (2 years ×  
192 2 altitudes × 2 locations).

193 To quantify the import of tropospheric O<sub>3</sub> into Europe, for each trajectory, all the trajectory points  
194 were co-located with corresponding TOMCAT O<sub>3</sub> mixing ratio values (i.e. the horizontal and vertical  
195 grid box the trajectory point sits within and corresponding time stamp) and then the average O<sub>3</sub>-  
196 weighted back-trajectory (O<sub>3</sub>-WBT) determined (i.e. back-trajectories with larger O<sub>3</sub>WBT values  
197 come from air masses with larger O<sub>3</sub> content). This follows a similar approach to Graham et al.,  
198 (2020) and Stirling et al., (2020), though using a model chemical tracer and not emission inventories.

## 199 **3. Results**

### 200 **3.1 Surface Temperature**

201 Several studies (e.g. Li et al., 2020; Liu et al., 2020; Drouard et al., 2020) have documented the  
202 intense heat wave across Europe in the summer of 2018. This is further shown in **Figure 1** which  
203 compares surface temperature, co-retrieved with ozone and other variables from MetOp-A by the  
204 IMS scheme, between 2017 and 2018. In May, higher temperatures occur across Scandinavia (5.0-  
205 10.0 K), eastern Europe (3.0-7.0 K) and the UK (1.0-3.0 K), but temperatures are lower (-3.0 to -1.0 K)  
206 across Iberia. In June, a similar spatial distribution occurs but the magnitude of the differences is  
207 smaller. In July the largest temperature increases range from 6.0-8.0 K in Scandinavia to 2.0-6.0 K in  
208 the UK/France. Iberia continued to experience temperatures lower by -2.0 to 0.0 K. In August, there  
209 are near-zero differences over the UK, Iberia and most of Scandinavia but with increases of 1.0-3.0 K  
210 over eastern Europe and Finland.

### 211 **3.2 Satellite Ozone**

212 We investigate the longer-term variability in tropospheric O<sub>3</sub> (i.e. SCO<sub>3</sub>) to determine if 2017 is a  
213 suitable comparator for the 2018 summer O<sub>3</sub> enhancements as it is for temperature. **Figure 2** shows

214 the 2012-18  $\text{SCO}_3$  average between May and August for a domain over the Atlantic and Europe and  
215 the difference for the same season between specific years and the 2012-18 average. In 2012 and  
216 2013, there are significant positive differences from the average between 1.0 DU and 5.0 DU over  
217 much of the domain. Over continental Europe, the differences are smaller. Here, the significance of  
218 differences between the year-specific and long-term averages are determined using the Wilcoxon  
219 Rank test (Pirovano et al., 2012) at the 95% confidence level. In 2014 and 2015, there are negative  
220 differences across Europe (-4.0 DU to -1.0 DU). In 2016, similar negative differences are primarily  
221 across the north and south-east of the domain. In 2017, there are near-zero differences across the  
222 Atlantic, UK and western Europe. Over eastern Europe and Mediterranean, there are significant  
223 negative differences of between -2.0 DU and -1.0 DU. In 2018, across continental Europe there are  
224 significant positive differences between 2.0 DU and 4.0 DU. As the 2017 differences are relatively  
225 small in magnitude with a low proportion of significant pixels (i.e. Sig Pixels % = 32.7 is the lowest  
226 across the 7 years), it is representative of average conditions for comparison with 2018. For 2018,  
227 the summer  $\text{SCO}_3$  enhancements across continental Europe are the largest for the years shown with  
228 a coherent cluster of significant differences. This illustrates that the summer 2018  $\text{SCO}_3$   
229 enhancements are a substantial deviation from the average conditions (which we represent as 2017  
230 hereon) and that this is an intense  $\text{O}_3$  event.

231 Investigation of  $\text{SCO}_3$  retrieved from both GOME-2 (**Figure 3**) and the IMS scheme (**Figure 4**) show  
232 consistent enhancements in summer 2018. In 2017, between May and August, GOME-2 typically  
233 observed  $\text{SCO}_3$  values between 20.0-30.0 DU across continental Europe. Peak  $\text{SCO}_3$  values occurred  
234 over the Mediterranean (30.0-38.0 DU); relatively high ozone is a typical feature of the  
235 Mediterranean in summer (Richards et al., 2013). In 2018, the seasonality is consistent with 2017,  
236 but the continental European  $\text{SCO}_3$  values ranged between 25.0 DU and 35.0 DU. For the 2018-2017  
237 difference,  $\text{SCO}_3$  enhancements occur across continental Europe in all four months but peaked in  
238 May and July between 3.0 DU and 8.0 DU, while typically 1.0-5.0 DU in June and August. The spatial  
239 distribution of IMS-retrieved  $\text{SCO}_3$  is similar to that of GOME-2 in 2017 and 2018, although the  
240 absolute values tend to be systematically lower by 3.0-4.0 DU. However, despite this systematic  
241 offset, the 2018-2017 differences are reasonably consistent with GOME-2. Across continental  
242 Europe, IMS  $\text{SCO}_3$  shows 2018 enhancements in all months investigated, but peaks in May and July,  
243 like GOME-2, between 3.0 DU and 6.0 DU. The differences range from 1.0 DU to 3.0 DU in June and  
244 are approximately 1.0 DU in August (though a peak enhancement of 3.0-5.0 DU occurs over the  
245 Mediterranean). Spatial correlations between the GOME-2 and IASI difference (i.e. 2018-2017) maps  
246 for the months investigated ranged between 0.21 and 0.47 (see **SM 5**).

247 The GOME-2 and IASI instruments observe UV-Vis and IR wavelengths, with peak vertical sensitivities  
248 to tropospheric  $\text{O}_3$  in the lower and mid/upper troposphere, respectively. Consistency in the 2018  
249 enhancements in  $\text{SCO}_3$  indicates that these extend over the bulk of the troposphere and increases  
250 confidence in the detected enhancements for both sensors.

251 Investigation of several satellite-retrieved  $\text{O}_3$  precursor gases (see **SM 2**) showed enhancements in  
252 total column methanol ( $\text{TCCH}_3\text{OH}$ , **Figure S2**), especially linked to May and July temperature  
253 enhancements (**Figure 1**), minor increases in tropospheric column  $\text{NO}_2$  ( $\text{TCNO}_2$ , **Figure S3**) in May and  
254 July over central Europe and widespread enhancements (weakest in July and strongest in August) in  
255 total column carbon monoxide ( $\text{TCCO}$ , **Figure S4**). Investigation of the GOME-2 and IASI total column  
256  $\text{O}_3$  ( $\text{TCO}_3$ ) differences between 2017 and 2018 (**Figures S5 & S6**) showed these to be in close  
257 agreement. Some spatial structure is similar to that of the  $\text{SCO}_3$  difference patterns (**Figures 3 and**

258 4), with correlations of approximately 0.5 between TCO<sub>3</sub> and SCO<sub>3</sub> for each instrument (see **SM 3**).  
259 Given the complex relationship between tropospheric O<sub>3</sub>, precursor gases, atmospheric chemistry  
260 (e.g. NO<sub>x</sub> or VOC-limited regimes), surface deposition and meteorological conditions (e.g.  
261 atmospheric temperatures and transport), a detailed chemistry transport model is required to assess  
262 the key processes leading to the observed SCO<sub>3</sub> enhancements over Europe.

### 263 3.3 Surface Ozone

264 Increased temperatures during heat waves have been shown to enhance surface O<sub>3</sub> concentrations  
265 (e.g. Jacob and Daniel, 2009; Vieno et al., 2010; Pyrgou et al., 2018). In the summer (May-June-July-  
266 August, MJJA) of 2018, EMEP recorded larger O<sub>3</sub> mixing ratios across most of Europe in comparisons  
267 to 2017 (**Figure 5a & b**). Over central Europe, surface O<sub>3</sub> mixing ratios ranged from approximately  
268 45.0 ppbv to over 60.0 ppbv, while in 2017 it was 35.0 ppbv to 50.0 ppbv. Over the UK and north-  
269 western Europe, surface O<sub>3</sub> mixing ratios ranged from 20.0 ppbv to 30.0 ppbv and then 25.0 ppbv to  
270 35.0 ppbv in MJJA 2017 and 2018, respectively. In Scandinavia and eastern Europe, surface O<sub>3</sub> mixing  
271 ratios ranged from 20.0 ppbv to 35.0 ppbv in MJJA 2017, while increasing to 25.0 ppbv to  
272 approximately 40.0 ppbv in MJJA 2018. **Figure 5c** highlights these widespread enhancements where  
273 domain-average surface O<sub>3</sub> mixing ratios are larger by typically 5.0-10.0 ppbv in May and from mid-  
274 June to mid-August in 2018. **Figure 5d** shows that the domain median surface O<sub>3</sub> concentration  
275 across MJJA was larger by 2.0-3.0 ppbv in 2018, but the 2018 extremes were greater with 75<sup>th</sup> and  
276 95<sup>th</sup> percentiles of 45.0 ppbv and 55.0 ppbv in 2017 and 48.0 ppbv and 59.0 ppbv in 2018. Therefore,  
277 surface observations of O<sub>3</sub> recorded widespread enhancements in MJJA 2018 compared to 2017  
278 with peak site differences >10.0 ppbv. This is generally consistent with the 2018 layer-averaged  
279 enhancements in the satellite-retrieved SCO<sub>3</sub> for regions where both datasets have spatial coverage.

### 280 3.4. Model Simulations

281 We use the TOMCAT model to investigate different factors potentially driving the observed  
282 enhancements in tropospheric O<sub>3</sub>. In comparisons with the observations (see **SM 5**) the model  
283 reproduces the sign and spatial distribution of observed 2018-2017 differences reasonably well.  
284 Although it has a tendency to underestimate the absolute magnitude, we are confident in the  
285 model's ability to simulate the tropospheric O<sub>3</sub> enhancements relative to 2017.

286 At the surface (**Figure 6**), TOMCAT CTL\_DIFF (i.e. Met18\_Emis18 - Met17\_Emis17) suggests that O<sub>3</sub> is  
287 enhanced in May over Scandinavia (2.0- >5.0 ppbv), north-western Europe (0.0-2.0 ppbv), the Arctic  
288 Ocean (>5.0 ppbv) and off the coast of Iberia (3.0-5.0 ppbv). However, negative values exist over  
289 eastern Europe (-3.0 ppbv to -1.0 ppb) and the Atlantic west of Ireland (-3.0 ppbv to -1.0 ppb). In  
290 June, the negative differences persist in eastern Europe (-3.0 ppbv to -1.0 ppb), but positive  
291 differences are located over northern Scandinavia (1.0-2.0 ppbv) and the North Atlantic (2.0-4.0  
292 ppbv). For July, CTL\_DIFF shows the largest enhancements over continental Europe (i.e. Po Valley,  
293 France, Benelux region and Iberia) and the UK (>5.0 ppbv). Negative differences of between -3.0  
294 ppbv and -1.0 ppbv remain over eastern Europe. In August, the only clear differences are over Iberia  
295 and the western Mediterranean, ranging between 3.0 ppbv and >5.0 ppbv. Overall, TOMCAT  
296 simulates sub-regional surface O<sub>3</sub> enhancements over Europe, which are generally consistent with  
297 EMEP observations apart from several sites over eastern Europe.

298 At 500 hPa, TOMCAT CTL\_DIFF shows larger-scale O<sub>3</sub> enhancements in 2018 compared to 2017 (>5.0  
299 ppbv) throughout May to August. In May and August, there are, however, a few negative differences

300 (-5.0 ppbv to -3.0 ppbv) over far eastern Europe. In June and July, the full domain is more or less  
301 dominated by O<sub>3</sub> enhancements in 2018. In **Figures 3** and **4** (and **SM 5**), GOME-2 and IASI (and  
302 TOMCAT with the instrument averaging kernels (AKs) applied to account for the vertical sensitivity of  
303 the retrievals, see **SM 5** for more information) show SCO<sub>3</sub> enhancements during these months of  
304 2018. Given the vertical extents and peak heights of their retrieval sensitivities and consistency in  
305 spatial patterns (**Figs SM 9** and **11**) it is evident that the O<sub>3</sub> enhancements detected by GOME-2 and  
306 IASI extend over the free troposphere. The model shows large-scale O<sub>3</sub> enhancements in the free  
307 troposphere and similar patterns to GOME-2 and IASI when averaging kernels applied. So, the model  
308 corroborates this finding from the satellite retrievals. Signals from EMEP and TOMCAT at the surface,  
309 on the other hand, are more mixed across the domain.

310 The right-hand column of **Figure 6** shows the relative difference in the stratospheric O<sub>3</sub> contribution  
311 to the 500 hPa O<sub>3</sub> layer (i.e. Strat % @ 500 hPa), from CTL\_DIFF, between 2017 and 2018. Here, the  
312 percentage of stratospheric O<sub>3</sub> contributing to the O<sub>3</sub> concentration at the 500 hPa is calculated for  
313 2017 and 2018 and then the 2018-2017 difference determined. The largest enhancement to the 500  
314 hPa layer was in July where the stratospheric O<sub>3</sub> contribution increased by 3.0% to >5.0% across  
315 Europe. In June and August, the spatial patterns are similar with stratospheric O<sub>3</sub> contribution  
316 enhancements of 3.0-5.0% across southern Europe, Scandinavia and the North Atlantic (above the  
317 UK). In the North Atlantic, UK and northern Europe, there are near-zero changes in June and August.  
318 In May, there are enhancements >5.0% across the northern region of the domain and northern  
319 Africa, while smaller enhancements (1.0%-3.0%) over the UK and near-zero changes over eastern  
320 Europe. This is partially supported by analysis of TCO<sub>3</sub> (see **SM 3**) where there are reasonable spatial  
321 correlations (~0.5 to 0.6) between the SCO<sub>3</sub> 2017-2018 summer differences and the equivalent for  
322 TCO<sub>3</sub>. Therefore, these results indicate a potentially enhanced contribution of stratospheric O<sub>3</sub> into  
323 the mid-troposphere during the summer of 2018 across Europe.

324 To quantify the separate importance of precursor emissions and meteorology in governing the  
325 summer 2018 O<sub>3</sub> enhancements we compare the sensitivity experiments with the control runs.  
326 **Figure 7** (left column) shows the results for the fixed emissions differences (i.e. FIXED\_EMIS\_DIFF)  
327 between years (i.e. Met18\_Emis17 – Met17\_Emis17). At the surface, the FIXED\_EMIS\_DIFF show  
328 similar spatial patterns to that of CTL\_DIFF (**Figure 6** – left column). The domain spatial difference  
329 correlations between these simulations is greater than 0.96 for all months considered. However,  
330 FIXED\_EMIS\_DIFF (**Figure 7** - left column) tends to be lower than CTL\_DIFF (**Figure 6** – left column)  
331 by approximately 0.0-2.9 ppbv (i.e. positive red regions are weaker and negative blue regions  
332 stronger in intensity). Therefore, the Met18\_Emis17 run struggles to reproduce the absolute surface  
333 O<sub>3</sub> enhancements in the Met18\_Emis18 run. When the fixed meteorology differences  
334 (FIXED\_MET\_DIFF, i.e. Met18\_Emis18 - Met18\_Emis17, **Figure 8** - left column) are compared with  
335 CTL\_DIFF, the surface 2018-2017 differences are substantially different.

336 Surface FIXED\_MET\_DIFF ranges between 0.0 ppbv and 2.0 ppbv across the domain in May and June  
337 and is more confined to continental Europe in July and August. This shows that TOMCAT simulates  
338 lower 2018 summer-time O<sub>3</sub> when 2017 emissions are used and indicates that emissions do have  
339 some role in controlling O<sub>3</sub> levels at the surface. However, as the spatial difference pattern for  
340 FIXED\_MET\_DIFF (**Figure 8** – left column) is different to that of CTL\_DIFF (**Figure 6** – left column),  
341 spatial correlations between them range from -0.53 to 0.54 over the four months, it suggests that  
342 meteorology is important in governing the spatial distribution of CTL\_DIFF. This is supported by the  
343 fact that FIXED\_MET\_DIFF - CTL\_DIFF (**Figure 8** left column – **Figure 6** left column) yields absolute



344 domain variations between 0.0 ppbv and 12.2 ppbv. Therefore, the two sensitivity experiments  
345 suggest meteorology and emissions both play important roles in controlling surface O<sub>3</sub> during the  
346 summer of 2018, but meteorology predominantly governs the spatial pattern and absolute  
347 magnitude of the O<sub>3</sub> enhancements.

348 At 500 hPa, comparison of FIXED\_EMIS\_DIFF and CTL\_DIFF show very consistent spatial patterns  
349 across the four months with correlations all above 0.98. In terms of the absolute differences  
350 between FIXED\_EMIS\_DIFF and CTL\_DIFF (i.e. **Figure 7** centre column – **Figure 6** centre column) it  
351 peaks at approximately 2.8 ppbv. For FIXED\_MET\_DIFF, the spatial correlation with CTL\_DIFF, as for  
352 the surface, is variable with values between -0.38 and 0.43. The absolute differences between  
353 FIXED\_MET\_DIFF and CTL\_DIFF (i.e. **Figure 8** centre column – **Figure 6** centre column) ranges from  
354 0.0 ppbv to 14.8 ppbv. Therefore, emissions have a secondary role in controlling the O<sub>3</sub> while  
355 meteorology is by far the dominant factor. For Strat % @ 500 hPa, the spatial correlations between  
356 CTL\_DIFF and FIXED\_EMIS\_DIFF are above 0.95 for all months and the absolute differences between  
357 them (i.e. **Figure 7** right column - **Figure 6** right column) are near-zero. Comparison of  
358 FIXED\_MET\_DIFF and TC\_CTL shows spatial difference correlations ranging between -0.33 and 0.71  
359 and absolute differences (i.e. **Figure 8** right column - **Figure 6** right column) peaking at 12.9%.  
360 Therefore, as expected, meteorological processes are dominating the influence of the stratospheric  
361 O<sub>3</sub> contribution (i.e. through stratosphere-troposphere exchanges) to the 500 hPa layer during the  
362 summer 2018 O<sub>3</sub> enhancements over Europe.

363 To investigate the importance of stratospheric-troposphere exchange to the middle troposphere  
364 enhancement (i.e. as shown in the TOMCAT 500 hPa layer and the satellite SCO<sub>3</sub> data), **Figures 9** and  
365 **10** show TOMCAT control run zonal 2018-2017 difference cross-sections (for the domain longitudes)  
366 of O<sub>3</sub> profiles and the stratospheric O<sub>3</sub> contribution to each pressure layer. In May and June, in the  
367 lower troposphere (approximately surface to 800 hPa), there are negative (-3.0% to 0.0%) and  
368 positive (0.0% to 3.0%) differences between 30-50°N and 50-70°N, respectively. During June, there  
369 are positive differences (0.0% to 5.0%) across most latitudes and in August, the opposite occurs to  
370 that of May/June. In the mid-troposphere (800-300 hPa), positive differences occur in most months  
371 (0.0-5.0% in May, 0.0-7.0% in June, >10% in July and 5.0-10.0% in August), though in May and August  
372 negative differences (-5.0% to 0.0%) exist around 40°N and 55°N. This is consistent with the 500 hPa  
373 O<sub>3</sub> differences in **Figure 6** (centre panels). In the upper troposphere – lower stratosphere (UTLS,  
374 approximately 300-100 hPa) there are limbs of positive O<sub>3</sub> differences (i.e. >10%, 5.0-10.0 ppbv)  
375 propagating into the mid-troposphere (30-40°N in May, 30-50°N in June, 40-50°N in July and 30-40°N  
376 & 60-70°N in August), suggestive of stratospheric intrusion into the mid-troposphere. Using the  
377 stratospheric O<sub>3</sub> tracer in TOMCAT, **Figure 10** shows the enhanced proportion of O<sub>3</sub> originating from  
378 the stratosphere in the summer of 2018. Interestingly, for all months (apart from May between 30-  
379 45°N), there are enhanced contributions of stratospheric O<sub>3</sub> (15.0% to >50.0%) in the lower-mid  
380 troposphere (i.e. below 500 hPa). In absolute terms, this is only a minor contribution typically <1.0  
381 ppbv below 800 hPa. Between 800-400 hPa, this increases to 1.0-5.0 ppbv (remains relatively  
382 consistent in percentage terms) in most months and latitude bands. In the UTLS, it increases to 5.0-  
383 10.0% enhancements in stratospheric O<sub>3</sub> contributions, which is consistent with its proximity to the  
384 stratosphere. In comparison between **Figures 9** and **10**, where there are enhancements in the  
385 stratospheric O<sub>3</sub> contribution but negative differences in O<sub>3</sub> (e.g. in June in the lower troposphere  
386 between 50°N and 55°N) which is suggestive of different processes influencing the O<sub>3</sub> concentrations  
387 (e.g. descent of relatively small stratospheric O<sub>3</sub> contributions but advection of tropospheric O<sub>3</sub> away

388 from the region). Overall though, in the mid-troposphere, where there are larger enhancements in  
389 O<sub>3</sub>, there are similar responses in the stratospheric O<sub>3</sub> contribution. For June, the mid-troposphere  
390 O<sub>3</sub> enhancement is approximately 5.0-7.0 ppbv with a signal of 1.0-2.0 ppbv in the stratospheric  
391 tracer. Therefore, in the more extreme cases, the stratospheric O<sub>3</sub> contribution is approximately  
392 15.0-40.0% to the mid-tropospheric O<sub>3</sub> enhancements in summer 2018 over Europe. However, a  
393 separate study would be required to undertake a detailed assessment of the meteorological  
394 processes controlling the enhanced stratospheric intrusion of ozone in the summer of 2018 and how  
395 it compares to other years (how does it compare with years other than 2017).

396 The two remaining factors, linked to meteorological processes (as suggested above), which may  
397 affect the O<sub>3</sub> enhancements in 2018 are increased summer temperatures (e.g. through enhanced  
398 kinetic rates), and the import of tropospheric O<sub>3</sub> from upwind (e.g. North America from the  
399 prevailing winds). **Figure 11** shows the 2017-2018 zonal temperature differences (i.e. same as **Figure**  
400 **9** but for temperature) with the correlation between the 2017 and 2018 temperature and O<sub>3</sub>  
401 differences overplotted. Qualitatively, the zonal differences in O<sub>3</sub> and temperature have some  
402 similarities. There are positive differences (temperature differences of 0.0-1.0%) between 50-60°N at  
403 the surface and 400 hPa in May and June. Then in July, collocated positive differences (peaking at  
404 2.0% or 3.0 K) exist between 50-70°N from the surface to 300 hPa. In August, there is no clear  
405 relationship between temperature and O<sub>3</sub> enhancements. In all months (to a lesser extent in  
406 August), in the UTLS, there are spatial agreements with positive differences between approximately  
407 30-45°N and negative differences between 50/55-70°N. In terms of correlations (i.e. temporal  
408 correlation in each grid box using the TOMCAT 6-hourly time series), the spatial agreement is  
409 relatively weak. In all months, most of domain has relatively small values ranging between -0.5 to  
410 0.5. There are only a few locations with strong correlations (i.e. > 0.5), which are in the UTLS or in  
411 the lower-mid troposphere between 50-70°N (June & August) and 45-55°N in July near the surface.  
412 Overall, the relationship between increased temperatures and enhanced kinetic rates yielding more  
413 ozone formation is non-linear, so it is unsurprising that the direct comparisons of temperature and  
414 ozone 2018-2017 differences above shows no clear pattern. Therefore, future work could include a  
415 further sensitivity experiment running TOMCAT for 2018, but with 2017 temperatures used in the  
416 chemistry routines to quantify the role of temperature in the summer 2018 O<sub>3</sub> enhancements.

417 To investigate the potential advection of tropospheric O<sub>3</sub>-rich air masses into Europe we have used  
418 ROTRAJ back-trajectories to determine the O<sub>3</sub>WBTs (i.e. an indicator of air mass O<sub>3</sub> content). As  
419 shown in **SM 6**, there is large variability in the O<sub>3</sub>WBT values and spatial distribution (i.e. **Figures S13**  
420 **and 14**), so they have to be gridded onto the TOMCAT horizontal resolution (see **Figures S15 and 16**).  
421 While this approach does not directly account for the frequency of trajectory points in each grid box,  
422 **Figures S13 and S14** show there is widespread coverage across the North Atlantic. This results in  
423 >500 trajectory points near the receptor sites (i.e. Paris and Berlin), ~100 trajectory points around  
424 the edge of Europe and 25-50 trajectory points in the North Atlantic (not shown here). Overall, this  
425 spatial distribution is relatively consistent and does not change substantially between years (typically  
426 10%), thus this approach is suitable in this study. **Figure 12** shows the differences (2018-2017)  
427 between the gridded O<sub>3</sub>WBTs where the back-trajectories have been released at the surface from  
428 Paris (**Figure 12a**), at the surface from Berlin (**Figure 12b**), at approximately 500 hPa from Paris  
429 (**Figure 12c**) and at approximately 500 hPa from Berlin (**Figure 12d**). We selected Paris and Berlin as  
430 they are situated in central Europe where the summer 2018 O<sub>3</sub> enhancements have been observed  
431 while the surface and 500 hPa are the altitudes of primary focus in the modelling work.

432 At the surface, Paris and Berlin show consistent patterns. Over the North Atlantic (i.e. origin of the  
433 prevailing winds into Europe), there are typically negative  $O_3$ WBT values between -5.0 ppbv and -1.0  
434 ppbv suggesting that advection of  $O_3$  into Europe during the summer (i.e. May-August) was  
435 predominantly larger in 2017 and did not strongly contribute to the 2018 observed surface  $O_3$   
436 enhancements. Advection of  $O_3$ -rich air in 2018 did originate from Scandinavia into continental  
437 Europe, though the number of trajectories is relatively low (see **Figure S13**). As both locations show  
438 similar relationships, it provides confidence in this methodology. At 500 hPa, the 50-60°N spatial  
439 pattern is less defined with values typically between -5.0 and 5.0 ppbv for both locations. However,  
440 in the southern North Atlantic (30-50°N) there are positive differences of approximately 3.0-10.0  
441 ppbv for both release locations. Note that as free-tropospheric winds tend to have larger horizontal  
442 velocities, the back-trajectories generally start from further away closer to North America. Again,  
443 given the broad similarity in differences between both release locations, it provides confidence in  
444 this approach. Overall, our results indicate a larger transport of  $O_3$  to the surface of continental  
445 Europe in 2017, while at approximately 500 hPa the import of  $O_3$  into Europe is larger in 2018. Here,  
446 the positive differences originate from the southern North Atlantic (i.e. a larger range of locations,  
447 absolute values and homogeneous signal than the mixed differences between 50-60°N).

448 One potentially important factor is dry deposition of  $O_3$  to the land surface. Due to the heatwave,  
449 stress on the biosphere and the associated die back of vegetation could potentially reduce the  
450 efficiency of  $O_3$  deposition decreasing the  $O_3$  sink (i.e.  $O_3$  is more likely to deposit onto land covered  
451 by vegetation than bare soil). Investigation of the normalised difference vegetation index (NDVI),  
452 from the IMS scheme, between the summers of 2017 and 2018 did not highlight any spatially  
453 coherent changes (not shown here). As a result, there is no obvious large-scale spatial vegetation die  
454 back in 2018 due to the heatwave and thus the impact this would have on ozone deposition in  
455 TOMCAT. Therefore, we ran two further experiments where the bare soil fraction for each grid box  
456 over Europe was increased and decreased by 25% in summer 2018. This was to investigate the  
457 sensitivity of surface ozone deposition to changes in the land surface. For the increase in bare soil  
458 fraction there was a moderate systematic increase in European summer ozone by 0.0-1.5 ppbv (i.e.  
459 less ozone deposition). When the bare soil fraction was decreased by 25%, this yielded a small  
460 decrease in surface ozone by approximately 0.5 ppbv. Overall, a sizable level of vegetation die back  
461 would be required for decreased ozone dry deposition to substantially contribute to the summer  
462 2018 surface ozone enhancements.

#### 463 **4. Discussion and Conclusions**

464 The summer of 2018 produced an intense heatwave across most of Europe with a substantial impact  
465 on tropospheric temperatures, droughts, stress on vegetation and human mortality. Observations of  
466 surface temperature, precursor gases and total column  $O_3$  ( $TCO_3$ ) experienced enhancements in  
467 2018 relative to 2017. In this paper, we have demonstrated a strong enhancement in surface and  
468 tropospheric  $O_3$  during the heatwave between May and August 2018. The EMEP surface data  
469 suggest an average European enhancement, relative to 2017, peaking at approximately 10.0 ppbv in  
470 July and August. Investigation of lower tropospheric  $O_3$  (i.e. surface-450 hPa sub-column  $O_3$  –  $SCO_3$ )  
471 from the GOME-2 and IASI instruments also showed enhancements, peaking at 5.0-10.0 DU, relative  
472 to 2017. Analysis of the long-term GOME-2  $SCO_3$  record indicates 2017 to be a suitably  
473 neutral/average reference year and the enhancement in 2018 to be anomalously large. Our  
474 comparisons were therefore made between the summers of 2017 and 2018.

475 Consistency between the UV (GOME-2) and IR (IASI) sounders was important to our analysis because  
476 their vertical sensitivities peak in the lower and mid-upper troposphere, respectively. The similar  
477 patterns of SCO<sub>3</sub> enhancement detected by the two sounders therefore indicate that these extend  
478 over the bulk of the troposphere, supportive of surface/lower tropospheric ozone enhancements.  
479 This consistency also provides confidence that the complementary vertical sensitivities of GOME-2  
480 and IASI ozone retrievals could be exploited in further investigation of tropospheric ozone in the  
481 future (e.g. long-term trends from multiple platforms/retrieval schemes have shown large-scale  
482 inconsistencies in other studies e.g. Gaudel et al., (2018)).

483 Tropospheric O<sub>3</sub> behaviour is complex and the summer 2018 enhancements over Europe could  
484 potentially have been caused by various factors: atmospheric chemistry, meteorology (e.g.  
485 temperature, advection of O<sub>3</sub>-rich air masses), anthropogenic and natural precursor emissions, dry  
486 deposition and stratospheric intrusion. To investigate the interactions between these processes,  
487 potentially leading to the summer 2018 O<sub>3</sub> enhancements, we used the well-evaluated TOMCAT 3D  
488 CTM. Evaluation of the model in this study showed that it could accurately capture the spatial  
489 pattern, temporal evolution and sign (i.e. positive 2018-2017 O<sub>3</sub> differences) of the O<sub>3</sub>  
490 enhancements and that, although it underestimated the observed enhancements, TOMCAT is an  
491 adequate tool to investigate them.

492 The results of several model simulations showed that the surface ozone enhancements (mainly in  
493 north-western Europe) in the summer of 2018 were predominantly driven by meteorological  
494 processes with emissions acting as a secondary factor. As the ROTRAJ back-trajectories suggest that  
495 advection of summer-time O<sub>3</sub> was larger in 2017, the 2018 European O<sub>3</sub> enhancements at surface  
496 level were likely from in-situ processes. The TOMCAT stratospheric O<sub>3</sub> tracer indicated a negligible  
497 contribution of stratospheric O<sub>3</sub> to these surface enhancements. At 500 hPa, the enhancement in  
498 tropospheric O<sub>3</sub> is much larger spatially across Europe and dominated by meteorological processes.  
499 Intrusion of stratospheric O<sub>3</sub> into the mid-troposphere has a moderate influence on the  
500 observed/modelled O<sub>3</sub> enhancements with contributions of up to 15.0-40.0%. Correlations between  
501 TOMCAT temperature and O<sub>3</sub> enhancements show broad agreement at some latitudes (e.g. 50-70°N  
502 in the lower-mid troposphere). However, this relationship is non-linear and difficult to quantify  
503 without further simulations/model tracers, which was beyond the scope of this study. ROTRAJ back-  
504 trajectories suggest that in 2018, relative to 2017, there is the advection of more O<sub>3</sub>-rich airmasses  
505 into the European mid-troposphere contributing to the summer 2018 O<sub>3</sub> enhancements at this  
506 altitude. Therefore, in the summer of 2018 over Europe, in-situ meteorological processes appear to  
507 be predominantly driving surface O<sub>3</sub> enhancements over Europe, while advection of tropospheric O<sub>3</sub>-  
508 rich air and stratospheric intrusion are driving the corresponding tropospheric O<sub>3</sub> enhancements

509 Overall, through our study focusing on the European summer 2018 air pollution episode, we have  
510 demonstrated the use of novel satellite datasets and a modelling framework (i.e. targeted sensitivity  
511 experiments and model tracers) suitable to investigate the air quality impacts from future European  
512 heatwaves such as that which occurred in summer 2022.

### 513 **Acknowledgements**

514 This work was funded by the UK Natural Environment Research Council (NERC) by providing funding  
515 for the National Centre for Earth Observation (NCEO, award reference NE/R016518/1).

### 516 **Conflicting Interests**

517 The authors declare that they have no conflicts of interest.

518

### 519 **Date Availability**

520 The TOMCAT simulations are publicly available at

521 [http://homepages.see.leeds.ac.uk/~earrjpo/european\\_summer\\_2018\\_o3/tomcat](http://homepages.see.leeds.ac.uk/~earrjpo/european_summer_2018_o3/tomcat), while the RAL  
522 Space satellite can be found at

523 [http://homepages.see.leeds.ac.uk/~earrjpo/european\\_summer\\_2018\\_o3/satellite](http://homepages.see.leeds.ac.uk/~earrjpo/european_summer_2018_o3/satellite). The EMEP  
524 surface O<sub>3</sub> data was obtained from <http://ebas-data.nilu.no/default.aspx>. The GOME-2 tropospheric  
525 column NO<sub>2</sub> data was downloaded from EUMETSAT at [https://acsaf.org/nrt\\_access.php](https://acsaf.org/nrt_access.php). The  
526 TOMCAT and RAL Space satellite data will be uploaded to the Zenodo open access portal  
527 (<https://zenodo.org/>) if this manuscript is accepted for publication in ACP after the peer-review  
528 process.

### 529 **Author Contributions**

530 RJP, MPC and BJK conceptualised and planned the research study. RJP performed the TOMCAT  
531 model simulations with support from MPC and WF. The JULES BVOC emissions were provided by ECP  
532 and GDH. RJP analysed the satellite data provided by RAL Space (BJK, RS, BGL and LJV) with support  
533 from BJK, RS and BGL. RJP undertook the EMEP analysis. RJP ran ROTRAJ with technical support from  
534 SRA and AMG. RJP prepared the manuscript with contributions from all co-authors.

### 535 **References**

536 Akritidis, D., Pozzer, A. and Zanis, P. 2019. On the impact of future climate change on tropopause  
537 folds and tropospheric ozone. *Atmospheric Chemistry and Physics*, **19**, 14387-14401, doi:  
538 10.5194/acp-19-14387-2019.

539 Archibald, A.T., et al. 2020. Description and evaluation of the UKCA stratosphere–troposphere  
540 chemistry scheme (StratTrop vn 1.0) implemented in UKESM1. *Geoscientific Model Development*, **13**,  
541 1223–1266, doi: 10.5194/gmd-13-1223-2020.

542 Bastos, A., Ciais, P., Friedlingstein, P., et al.: Direct and seasonal legacy effects of the 2018 heat wave  
543 and drought on European ecosystem productivity, *Science Advances*, **6**, eaba2724,  
544 doi:10.1126/sciadv.aba2724, 2020.

545 Best, M.J., Pryor, M., Clark, D.B., et al.: The Joint UK Land Environment Simulator (JULES), model  
546 description—Part 1: energy and water fluxes, *Geoscientific Model Development*, **4**, 677–699,  
547 doi:10.5194/gmd-4-677-2011, 2011.

548 Chipperfield, M.P.: New version of the TOMCAT/SLIMCAT off-line chemistry transport model:  
549 Intercomparison of stratospheric trace experiments, *Quarterly Journal of the Royal Meteorological*  
550 *Society*, **132**, 1179–1203, doi:10.1256/qj.05.51, 2006.

551 Churkina, G., Kuik, F., Bonn, B., et al. 2017. Effect of VOC Emissions from Vegetation on Air Quality in  
552 Berlin during a Heatwave. *Environmental Science and Technology*, **51**(11), 6120-6130, doi:  
553 10.1021/acs.est.6b06514.

554 Clark, D. B., Mercado, L.M., Sitch, S., et al.: The Joint UK Land Environment Simulator (JULES), model  
555 description—Part 2: carbon fluxes and vegetation dynamics, *Geoscientific Model Development*, **4**,  
556 701–722, doi:10.5194/gmd-4-701-2011, 2011.

557 Clerbaux, C., Boynard, A., Clarisse, L., et al.: Monitoring of atmospheric composition using the

558 thermal infrared IASI/MetOp sounder, *Atmospheric Chemistry and Physics*, 9 (16), 6041–6054,  
559 doi:10.5194/acp-9-6041-2009, 2009.

560 Dee, D.P., Uppala, S.M., Simmons, A.J., et al.: The ERA-Interim reanalysis: Configuration and  
561 performance of the data assimilation system, *Quarterly Journal of the Royal Meteorological Society*,  
562 137 (656), 553–597, doi:10.1002/qj.828, 2011.

563 Dirmeyer, P.A., Balsamo, G., Blyth, E.M., et al.: Land-Atmosphere Interactions Exacerbated the  
564 Drought and Heatwave Over Northern Europe During Summer 2018, *AGU Advances*, 2,  
565 e2020AV000283., doi: 10.1029/2020AV000283, 2020.

566 Doherty, R. M., Heal, M. R., and O’Connor, F. M.: Climate change impacts on human health over  
567 Europe through its effect on air quality, *Environmental Health*, 16(1), 33–44, doi:10.1186/s12940-  
568 017-0325-2, 2017.

569 Drouard, M., Kornhuber, K. and Woollings, T.: Disentangling Dynamical Contributions to Summer  
570 2018 Anomalous Weather Over Europe, *Geophysical Research Letter*, 46, 12537-12546,  
571 doi:10.1029/2019GL084601, 2020.

572 Emmons, L. K., Arnold, S. R., Monks, S. A., et al.: The POLARCAT Model Intercomparison Project  
573 (POLMIP): overview and evaluation with observations, *Atmospheric Chemistry and Physics*, 15, 6721–  
574 6744, doi:10.5194/acp-15-6721-2015, 2015.

575 Forster, P., Ramaswamy, V., Artaxo, P., et al.: Changes in Atmospheric Constituents and in Radiative  
576 Forcing, in: *Climate Change 2007: The Physical Science Basis. Contribution of Working Group I to the*  
577 *Fourth Assessment Report of the Intergovernmental Panel on Climate Change*, Cambridge University  
578 Press, Cambridge, United Kingdom and New York, NY, USA, 2007.

579 García-Herrera, R., Díaz, J., Trigo, R.M., et al. 2020. A Review of the European Summer Heat Wave of  
580 2003. *Critical Reviews in Environmental Science and Technology*, **40**(4), 267-  
581 306, doi:10.1080/10643380802238137. Gaudel, A., Cooper, O.R., Ancellet, G., et al.: Tropospheric  
582 Ozone Assessment Report: Present day distribution and trends of tropospheric ozone relevant to  
583 climate and global atmospheric chemistry model evaluation. *Elementa*, 6(39), 1-58,  
584 doi:10.1525/elementa.291, 2018.

585 Graham, A. M., Pringle, K. J., Pope, R. J., et al.: Impact of the 2019/2020 Australian megafires on air  
586 quality and health, *GeoHealth*, 5, e2021GH000454, doi:10.1029/2021GH000454, 2020.

587 Granier, C., Bessagnet, B., Bond, T., et al.: Evolution of anthropogenic and biomass burning emissions  
588 of air pollutants at global and regional scales during the 1980–2010 period, *Climatic Change*, 109,  
589 163-190, doi:10.1007/s10584-011-0154-1, 2011.

590 Guerreiro, S.B., Dawson, R.J., Kilsby, C., et al.: Future heat-waves, droughts and floods in  
591 European cities, *Environmental Research Letters*, 13, 034009, 10.1088/1748-9326, 2018.

592 Heal, M.R., Heaviside, C., Doherty, R.M., et al. 2013. Health burdens of surface ozone in the UK for a  
593 range of future scenarios. *Environment International*, 61, 36-44, doi:10.1016/j.envint.2013.09.010.

594 Hollaway, M.J., Arnold, S.R., Challinor, A. J. and Emberson, L.D: Intercontinental trans-boundary  
595 contributions to ozone-induced crop yield losses in the North Hemisphere, *Biogeosciences*, 9, 271–  
596 2929, doi: 10.5194/bg-9-271-2012, 2012.

597 Honrath, R.E., Owen, R.C., Val Martin, M., et al. 2004. Regional and hemispheric impacts of  
598 anthropogenic and biomass burning emissions on summertime CO and O<sub>3</sub> in the North Atlantic

599 lower free troposphere. *Journal of Geophysical Research: Atmospheres*, 109(D24), doi:  
600 10.1029/2004JD005147.

601 Jacob, D.J., and Winner, D.A.: Effect of climate change on air quality, *Atmospheric Environment*, 43  
602 (1), 51-63, doi:10.1016/j.atmosenv.2008.09.051, 2009.

603 Jerrett, M., Burnett, R.T., Pope, C.A., et al.: Long-term ozone exposure and mortality, *The New*  
604 *England Journal of Medicine*, 360 (11), 1085–1095, doi: 10.1056/NEJMoa0803894, 2009.

605 Kaiser, J.W., Hell, A., Andreae, M.O., et al.: Biomass burning emissions estimated with a global fire  
606 assimilation system based on observed fire radiative power, *Biogeosciences*, 9(1), 527–554, doi:  
607 10.5194/bg-9-527-2012, 2012.

608 Lhotka, O., Kysely, J. and Farda, A.: Climate change scenarios of heat waves in Central Europe and  
609 their uncertainties, *Theoretical and Applied Climatology*, 131, 1043-1054, doi: 10.1007/s00704-016-  
610 2031-3, 2017.

611 Li, M., Yao, Y., Simmonds, I., et al.: Collaborative impact of the NAO and atmospheric blocking on  
612 European heat waves, with a focus on the hot summer of 2018, *Environmental Research Letters*, 15,  
613 114003, doi:10.1088/1748-9326/aba6ad, 2020.

614 Liu, X., He, B., Guo, L., et al.: Similarities and differences in the mechanisms causing the European  
615 summer heat waves in 2003, 2010 and 2018, *Earth's Future*, e2019EF001386, doi:  
616 10.1029/2019EF001386, 2020.

617 Mann, G.W., Carslaw, K.S., Spracklen, D.V., et al.: Description and evaluation of GLOMAP-mode: A  
618 modal global aerosol microphysics model for the UKCA composition-climate model. *Geoscientific*  
619 *Model Development*, 3(2), 519–551, doi:10.5194/gmd-3-519-2010, 2010.

620 Matsueda, M.: Predictability of Euro-Russian blocking in summer of 2010, *Geophysical Research*  
621 *Letters*, 38, L06801, doi:10.1029/2010GL046557, 2011.

622 Methven, J., Arnold, S.R., O'Connor, F.M., et al.: Estimating photochemically produced ozone  
623 throughout a domain using flight data and a Lagrangian model, *Journal of Geophysical Research:*  
624 *Atmospheres*, 10 (D9), doi:10.1029/2002JD002955, 2003.

625 Miles, G.M., Siddans, R., Kerridge, B. J., Latter, B. G., and Richards, N. A. D.: Tropospheric ozone and  
626 ozone profiles retrieved from GOME-2 and their validation, *Atmospheric Measurement Techniques*,  
627 8, 385–398, doi:10.5194/amt-8-385-2015, 2015.

628 Monks, S.A., Arnold, S.R., Hollaway, M. J., et al.: The TOMCAT global chemistry transport model v1.6:  
629 Description of chemical mechanism and model evaluation, *Geoscientific Model Development*, 10 (8),  
630 3025–3057, doi:10.5194/gmd-10-3025-2017, 2017.

631 Morgenstern, O., Hegglin, M.I., Rozanov, E., et al.: Review of the global models used with phase 1 of  
632 the Chemistry-Climate Model Initiative (CCMI), *Geoscientific Model Development*, 10 (2), 639–671,  
633 doi:10.5194/gmd-10-639-2017, 2017.

634 Munro, R., Siddans, R., Reburn, W. J., and Kerridge, B. J.: Direct measurement of tropospheric ozone  
635 distributions from space, *Nature*, 392, 168–171, doi:10.1038/32392, 1998.

636 Pacifico, F., Harrison, S.P., Jones, C.D., et al.: Evaluation of a photosynthesis-based biogenic isoprene  
637 emission scheme in JULES and simulation of isoprene emissions under present-day climate  
638 conditions, *Atmospheric Chemistry and Physics*, 11, 4371–4389, doi:10.5194/acp-11-4371-2011,  
639 2011.

640 Palmer, P., I., Marvin, M., R., Siddans, R., et al.: Nocturnal survival of isoprene linked to formation  
641 of upper tropospheric organic aerosol, *Science*, 375 (6580), 562-566,  
642 doi:10.1126/science.abg4506.

643 Papanastasiou, D.K., Melas, D. and Kambezidis, H.D., 2015. Air quality and thermal comfort levels  
644 under extreme hot weather. *Atmospheric Research*, 152, 4-13, doi:  
645 10.1016/j.atmosres.2014.06.002.

646 PHE (Public Health England), PHE heatwave mortality monitoring, available at:  
647 [https://assets.publishing.service.gov.uk/government/uploads/system/uploads/attachment\\_data/file](https://assets.publishing.service.gov.uk/government/uploads/system/uploads/attachment_data/file/942648/PHE_heatwave_report_2018.pdf)  
648 [/942648/PHE\\_heatwave\\_report\\_2018.pdf](https://assets.publishing.service.gov.uk/government/uploads/system/uploads/attachment_data/file/942648/PHE_heatwave_report_2018.pdf) (last accessed 3<sup>rd</sup> February 2022), 2019.

649 Pimlott, M.A., Pope, R.P., Kerridge, B.J., et al.: Investigating the global OH radical distribution using  
650 steady-state approximations and satellite data. *Atmospheric Chemistry and Physics*, **22**, 10467-  
651 10488, doi: 10.5194/acp-22-10467-2022, 2022.

652 Pirovano, G., Balzarini, A., Bessagnet, B., et al.: Investigating impacts of chemistry and transport  
653 model formulation on model performance at European scale, *Atmospheric Environment*, 53, 93–109,  
654 doi:10.1016/j.atmosenv.2011.12.052, 2012.

655 Pope, R.J., Savage, N.H., Chipperfield, M.P., et al.: The influence of synoptic weather regimes on UK  
656 air quality: analysis of satellite column NO<sub>2</sub>, *Atmospheric Science Letters*, 15, 211– 217,  
657 doi:10.1002/asl22.492, 2014.

658 Pope, R.J., Butt, E.W., Chipperfield, M.P., et al.: The impact of synoptic weather on UK surface ozone  
659 and implications for premature mortality. *Environmental Research Letters*, **11**, 124004,  
660 doi:10.1088/1748-9326/11/12/124004, 2016.

661 Pope, R.J., Chipperfield, M.P., Arnold, S.R., et al. 2018. Influence of the wintertime North Atlantic  
662 Oscillation on European tropospheric composition: an observational and modelling study.  
663 *Atmospheric Chemistry and Physics*, **18**, 8389–8408, doi: 10.5194/acp-18-8389-2018.

664 Pope, R.J., Arnold, S.R., Chipperfield, M.P., et al.: Substantial Increases in Eastern Amazon and  
665 Cerrado Biomass Burning-Sourced Tropospheric Ozone. *Geophysical Research Letters*, 47 (3),  
666 e2019GL084143, doi:10.1029/2019GL084143, 2020.

667 Pope, R. J., Kerridge, B. J., Siddans, R., et al.: Large enhancements in southern hemisphere satellite-  
668 observed trace gases due to the 2019/2020 Australian wildfires, *Journal of Geophysical Research:*  
669 *Atmospheres*, 1–13, doi:10.1029/2021jd034892, 2021.

670 Pyrgou, A., Hadjinicolaou, P and Santamouris, M: Enhanced near-surface ozone under heatwave  
671 conditions in a Mediterranean island, *Scientific Reports*, 8, 9191, doi:10.1038/s41598-018-27590-z,  
672 2018.

673 RAL Space, Optimal Estimation Method retrievals with IASI, AMSU and MHS – Final Report Version  
674 5.2, available at: [http://cedadocs.ceda.ac.uk/1377/1/iasi\\_mhs\\_final\\_report\\_v5p2.pdf](http://cedadocs.ceda.ac.uk/1377/1/iasi_mhs_final_report_v5p2.pdf) (last accessed  
675 17/08/2020), 2015.

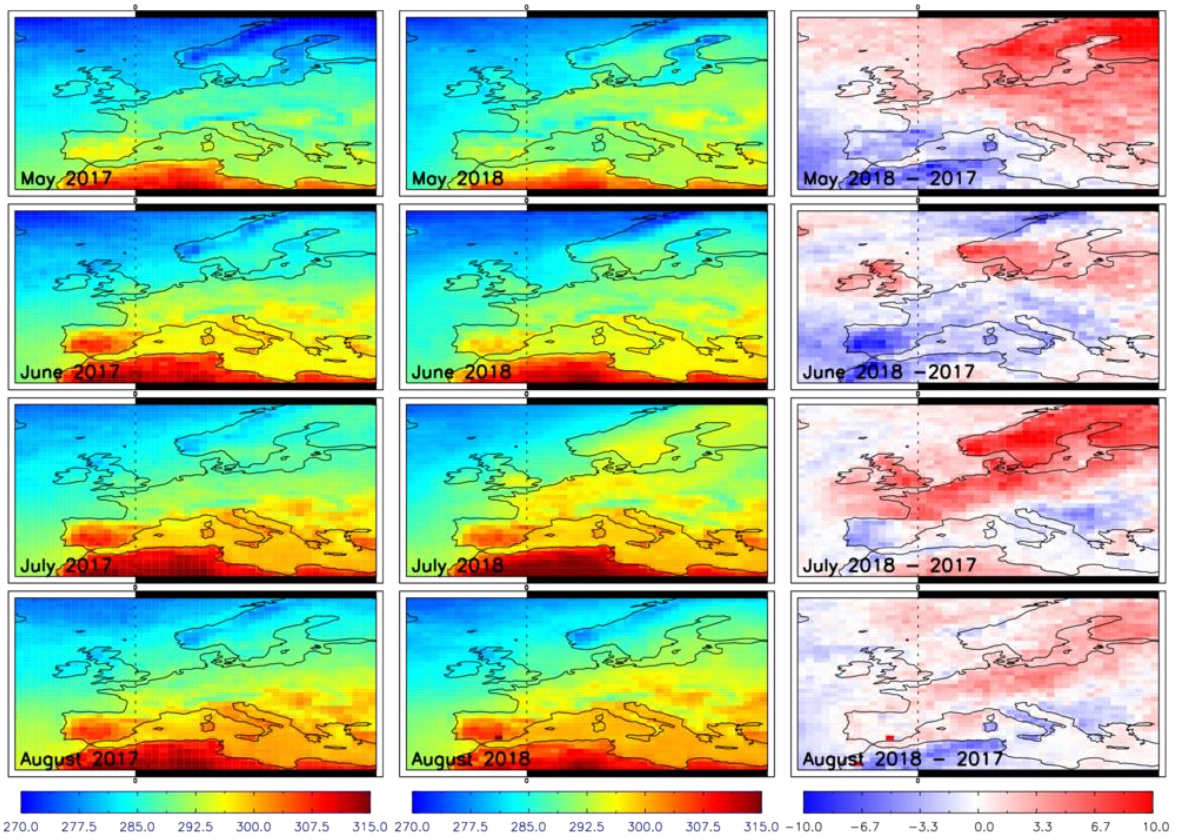
676 Rasilla, D., Allende, F., Martilli, A., et al. 2019. Heat Waves and Human Well-Being in Madrid (Spain).  
677 *Atmosphere*, 10(5), 288-309, doi: 10.3390/atmos10050288.

678 Rebetez, M., Dupont, O. and Giroud, M.: An analysis of July 2006 heatwave extent in Europe  
679 compared to the record year of 2003, *Theoretical and Applied Climatology*, 95, 1-7,  
680 doi:10.1007/s00704-007-0370-9, 2008.



- 681 Renneberg, H., Loreto, F., Polle, A., et al. 2006. Physiological Responses of Forest Trees to Heat and  
682 Drought. *Plant Biology*, **8**(5), 556-571, doi: 10.1055/s-2006-924084.
- 683 Richards, N.A.D, Arnold, S.R., Chipperfield, M.P., et al.: The Mediterranean summertime ozone  
684 maximum: global emission sensitivities and radiative impacts, *Atmospheric Chemistry and Physics*,  
685 **13**, 2231-2345, doi:10.5194/acp-13-2331-2013, 2013.
- 686 Riese, M., Ploeger, F., Rap, A., et al.: Impacts of uncertainties in atmospheric mixing on simulated  
687 UTLS composition and related radiative effects, *Journal of Geophysical Research: Atmospheres*, **117**,  
688 D16305, doi:10.1029/2012jd017751, 2012.
- 689 Rodgers, C.D.: Inverse methods for atmospheric sounding: Theory and practice. New Jersey, USA:  
690 World Science. 2000.
- 691 Roelofs, G.L., Kentarchos, A.S., Trickl, T., et al. 2003. Intercomparison of tropospheric ozone models:  
692 Ozone transport in a complex tropopause folding event. *Journal of Geophysical Research*, **108** (D12),  
693 8529, doi: 10.5194/acp-19-14387-2019.
- 694 Schultz, M.G., Schroder, S., Lyapina, O., et al. 2017. Tropospheric Ozone Assessment Report:  
695 Database and metrics data of global surface ozone observations. *Elementa – Science of the*  
696 *Anthropocene*, **5**(58), doi: 10.1525/elementa.244.
- 697 Scott, P.A., Stone, D.A. and Allen, M.R.: Human contributions to the European heatwave of 2003,  
698 *Nature*, **432**, 610-614, doi:10.1038/nature03089, 2004.
- 699 Sitch, S., Cox, P.M., Collins, W.J., & Huntingford, C.: Indirect radiative forcing of climate change  
700 through ozone effects on the land carbon sink, *Nature*, **448**, 791–795, doi:10.1038/nature06059,  
701 2007.
- 702 Smith, N.E., Kooijmans, L.M.J., Koren, G., et al.: Spring enhancements and summer reduction in  
703 carbon uptake during the 2018 drought in Northwestern Europe, *Philosophical Transactions B*, **375**,  
704 20190509, doi:10.1098/rstb.2019.0509, 2020.
- 705 Stockwell, D., Giannakopoulos, C., Plantevin, P.-H., et al. 1999. Modelling NO<sub>x</sub> from lightning and its  
706 impact on global chemical fields. *Atmospheric Environment*, **33**, 4477–4493, doi: 10.1016/S1352-  
707 2310(99)00190-9.
- 708 Thomas, M.A. and Devasthale, A.: Sensitivity of free tropospheric carbon monoxide to atmospheric  
709 weather states and their persistency: an observational assessment over the Nordic countries,  
710 *Atmospheric Chemistry and Physics*, **14**, 11545–11555, doi:10.5194/acp14-11545-2014, 2014.
- 711 Van Dingenen, R., Dentener, F.J., Raes, F., et al.: The global impact of ozone on agriculture crop  
712 yields under current and future air quality legislation. *Atmospheric Environment*, **43**(3), 604–618,  
713 doi:10.1016/j.atmosenv.2008.10.033, 2009.
- 714 Vieno, M., Dore, A.J., Stevenson, D.S., et al.: Modelling surface ozone during the 2003 heat-wave in  
715 the UK, *Atmospheric Chemistry and Physics*, **10**, 7963-7978, doi:10.5194/acp-10-7963-2010, 2010.
- 716 WHO (World Health Organisation), Ambient (outdoor) air pollution, available at:  
717 [https://www.who.int/news-room/fact-sheets/detail/ambient-\(outdoor\)-air-quality-and-health](https://www.who.int/news-room/fact-sheets/detail/ambient-(outdoor)-air-quality-and-health) (last  
718 accessed 3<sup>rd</sup> February 2022), 2021.
- 719 Yan, Y., Pozzer, A., Ojha, N., et al. 2018. Analysis of European ozone trends in the period 1995—  
720 2014. *Atmospheric Chemistry and Physics*, **18**(8), 5589—5605, doi: 10.5194/acp-18-5589-2018.

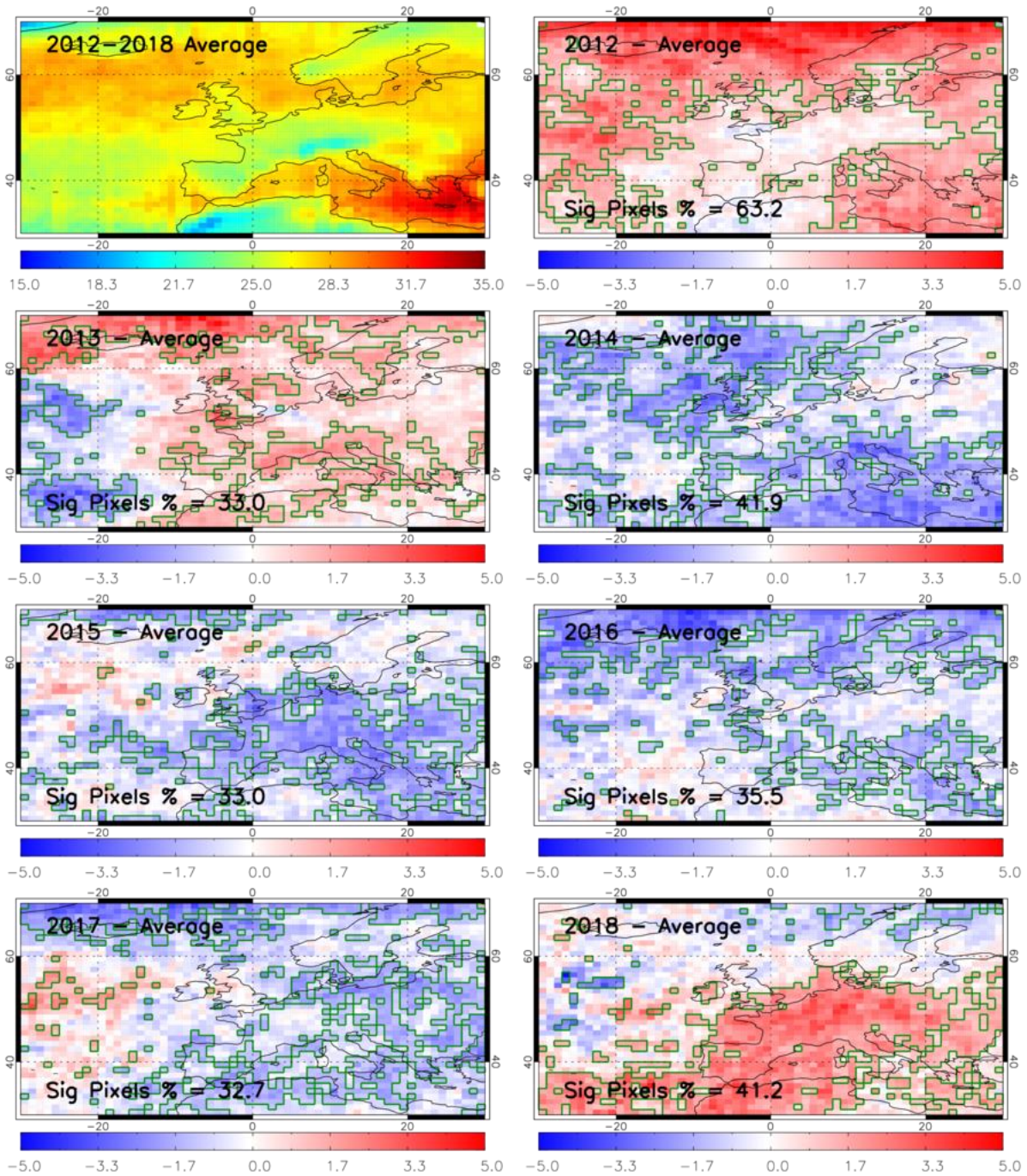
721 Figures:



722

723 **Figure 1:** Surface temperature (K) over Europe for May to August in 2017 (left column), 2018 (centre  
724 column) and 2018-2017 difference (right column) retrieved from MetOp-A IASI, MHS and AMSU by  
725 the IMS scheme.

726



727

728

729

730

731

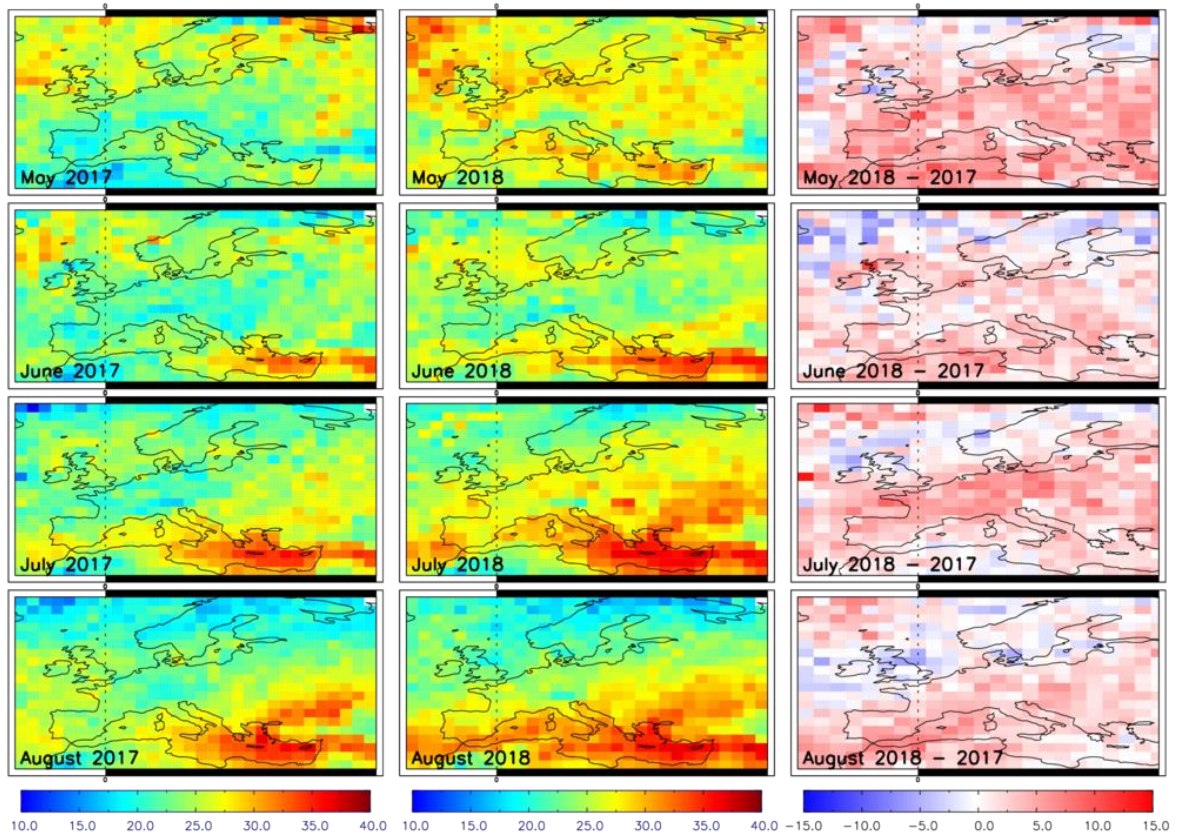
732

733

734

735

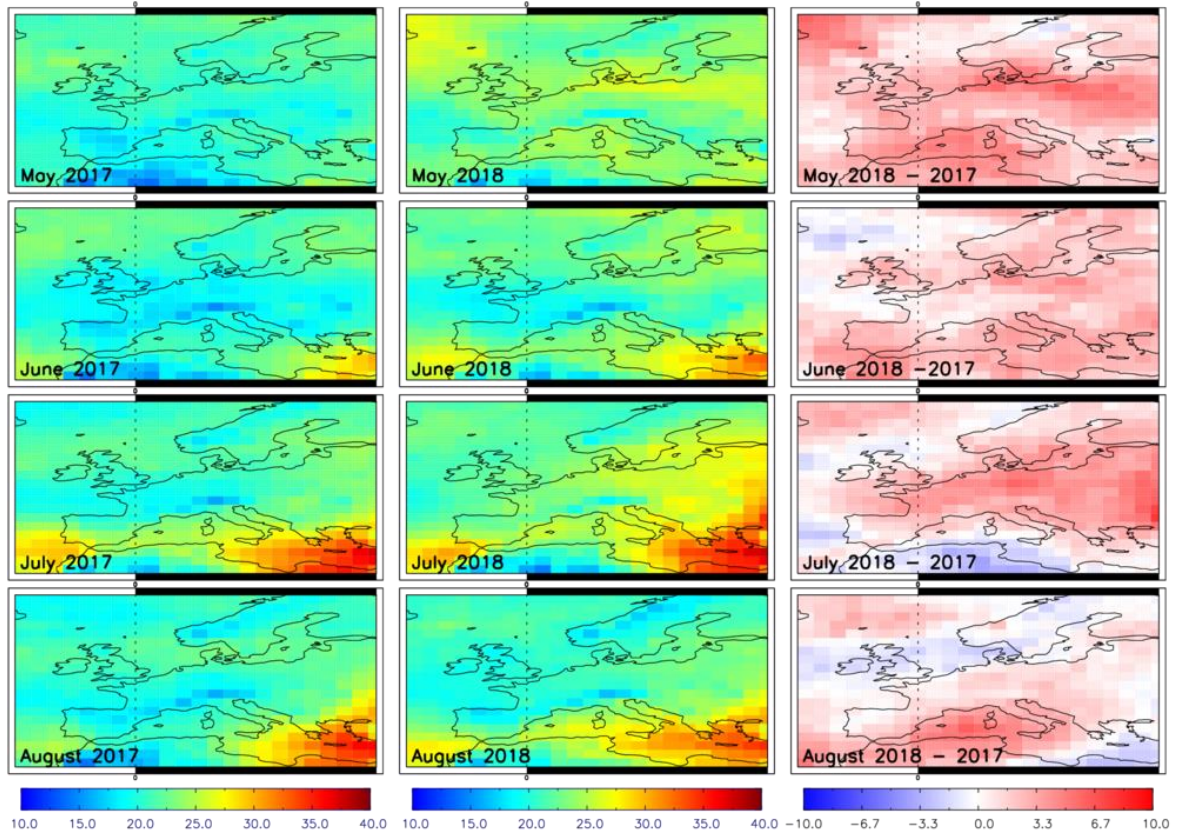
**Figure 2:** Sub-column ozone ( $SCO_3$ , surface-450 hPa), in Dobson units (DU), retrieved from GOME-2 on Metop-A averaged across May to August between 2012 and 2018 (top left panel) and the corresponding difference from the 2012-18 mean for each year, respectively. The green-polygon-outlined regions show where the year-specific seasonal average is significantly different (95% confidence level based on the Wilcoxon Rank Test (WRT)) from the long-term (2012-2018) seasonal average. The “Sig Pixel %” label indicates the number of pixels in the domain with significant differences.



736

737 **Figure 3:** SCO<sub>3</sub> (DU) from GOME-2 over Europe for May to August in (left column) 2017, (centre  
 738 column) 2018 and (right column) 2018-2017 difference.

739

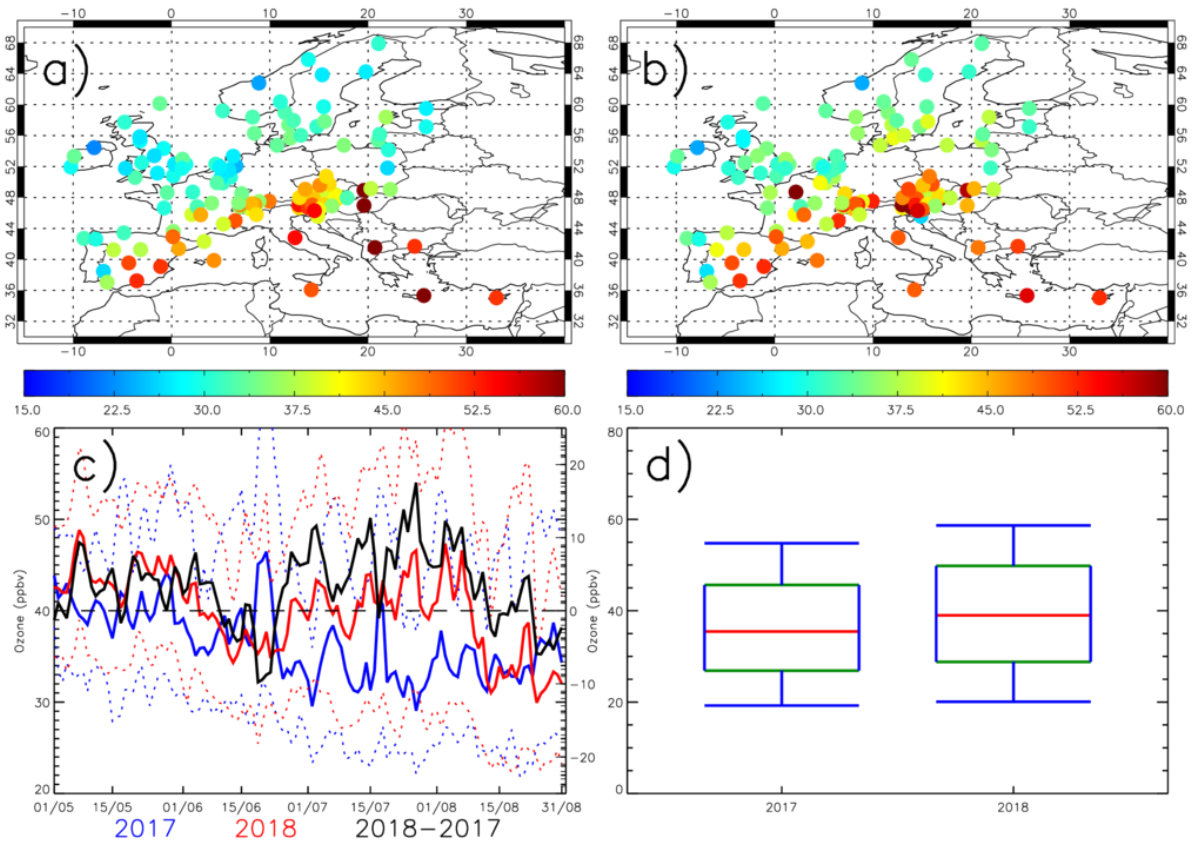


740

741 **Figure 4:** *SCO<sub>3</sub> (DU) for May to August in 2017 (left column), 2018 (centre column) and 2018-2017*  
 742 *difference (right column) over Europe retrieved from MetOp-A IASI, MHS and AMSU by the IMS*  
 743 *scheme.*

744

745



746

747

748

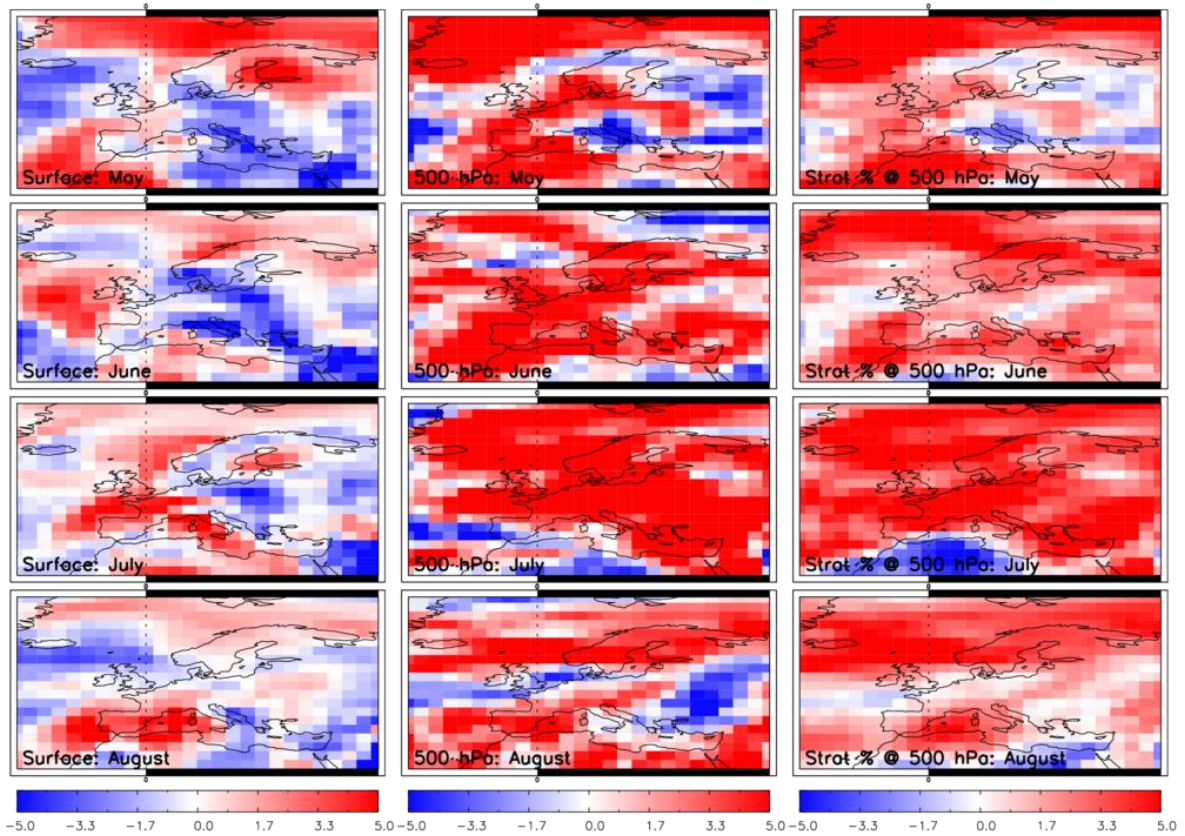
749

750

751

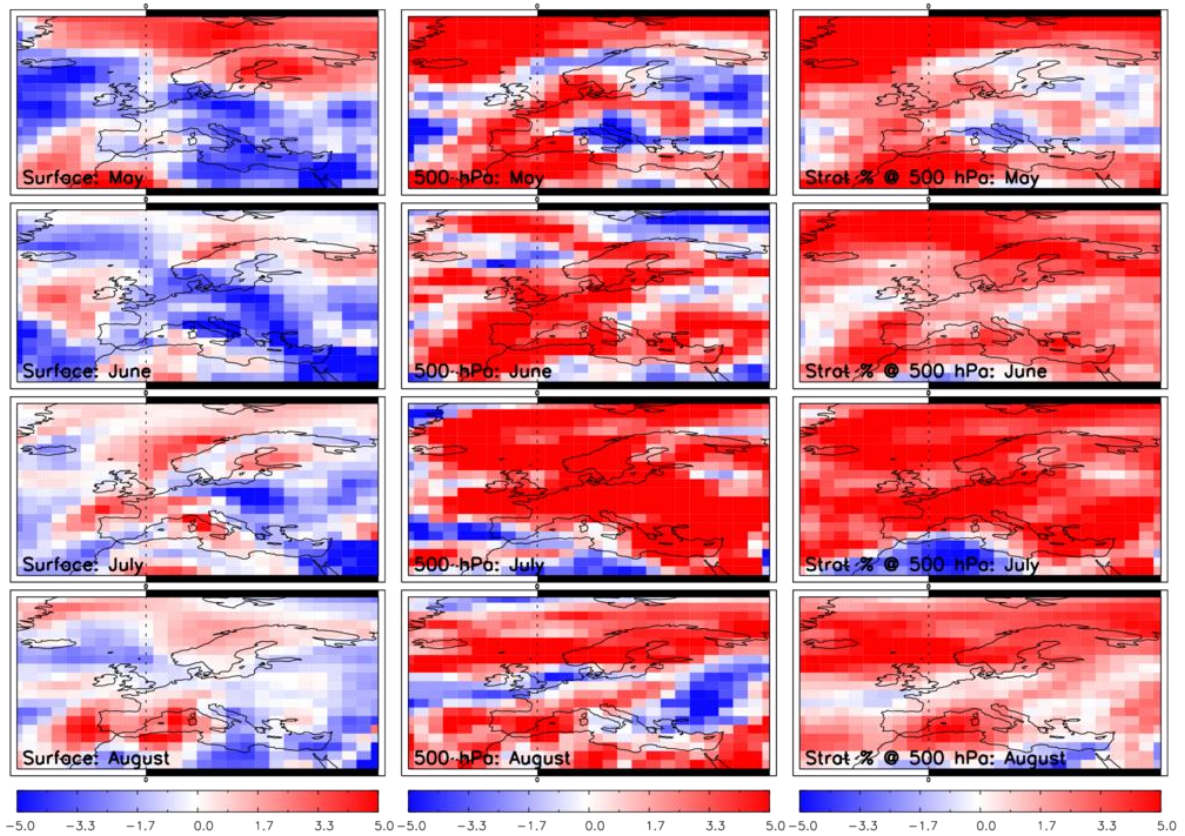
752

**Figure 5:** European surface ozone (ppbv) for a) May-June-July-August (MJJA) 2017, b) MJJA 2018), c) regional mean time series (dotted lines show mean  $\pm$  standard deviation) for MJJA 2017 (blue), MJJA 2018 (red) and the 2018-2017 difference (black) and d) box-whisker plots for MJJA 2017 and 2018. In panel d) the median, 25<sup>th</sup> & 75<sup>th</sup> percentiles and 10<sup>th</sup> & 90<sup>th</sup> percentiles are shown by the red, green and blue lines, respectively.



753  
 754  
 755  
 756  
 757

**Figure 6:** TOMCAT ozone (ppbv) 2018-2017 differences for May to August for the surface (left column), 500 hPa (centre column) and the stratospheric contribution (%) to the 500 hPa layer (right column).



758

759

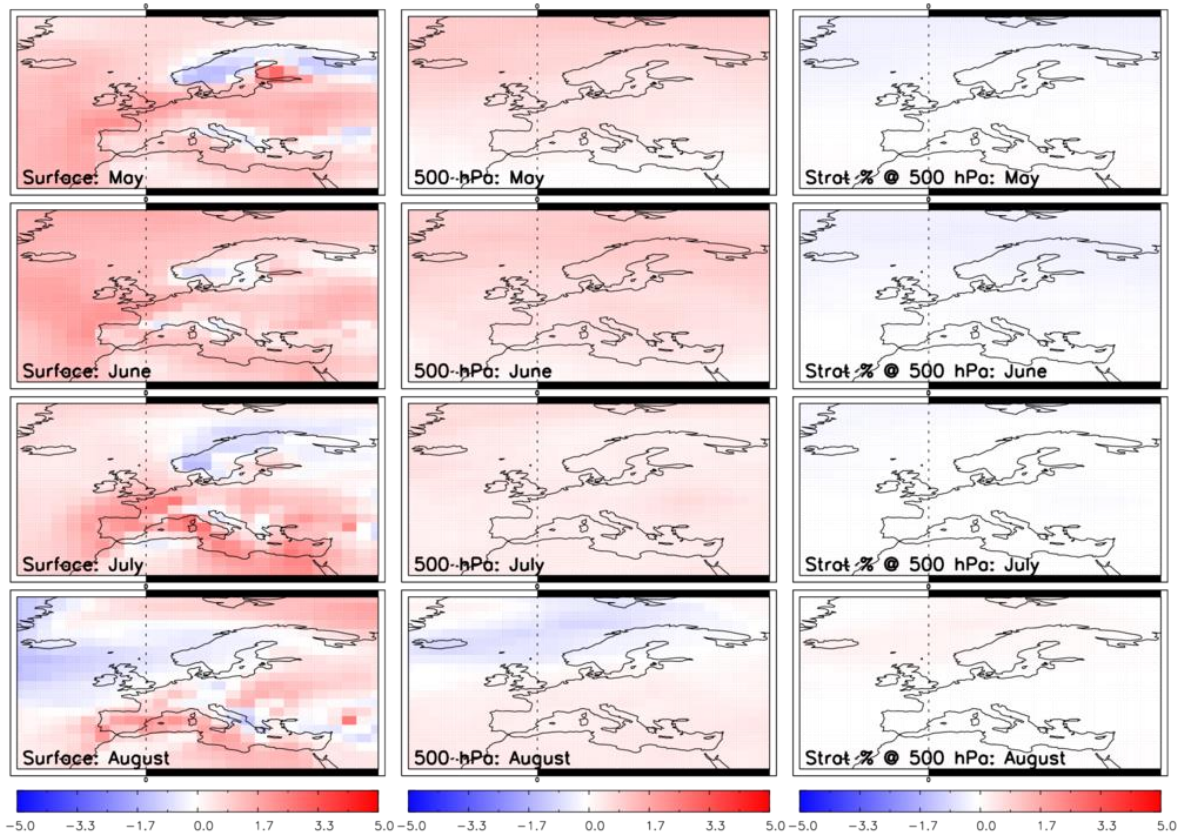
760

761

762

**Figure 7:** TOMCAT ozone (ppbv) 2018-2017 differences for May to August for the fixed emissions simulation (Fixed\_EMIS) for the surface (left column), 500 hPa (centre column) and the stratospheric contribution (%) to the 500 hPa layer (right column).





763

764

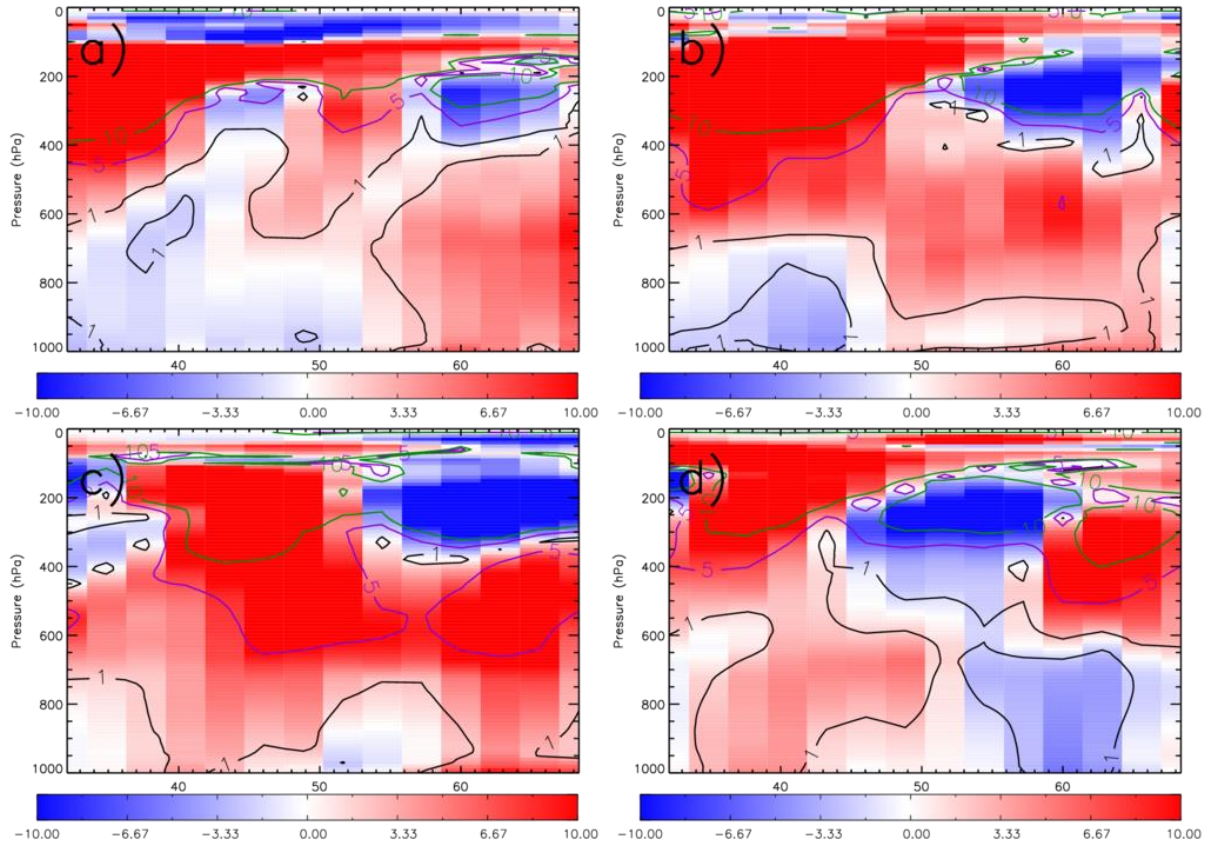
**Figure 8:** TOMCAT ozone (ppbv) 2018-2017 differences for May to August for the fixed meteorology simulation (Fixed\_MET) for the surface (left column), 500 hPa (centre column) and the stratospheric contribution (%) to the 500 hPa layer (right column).

767

768

769

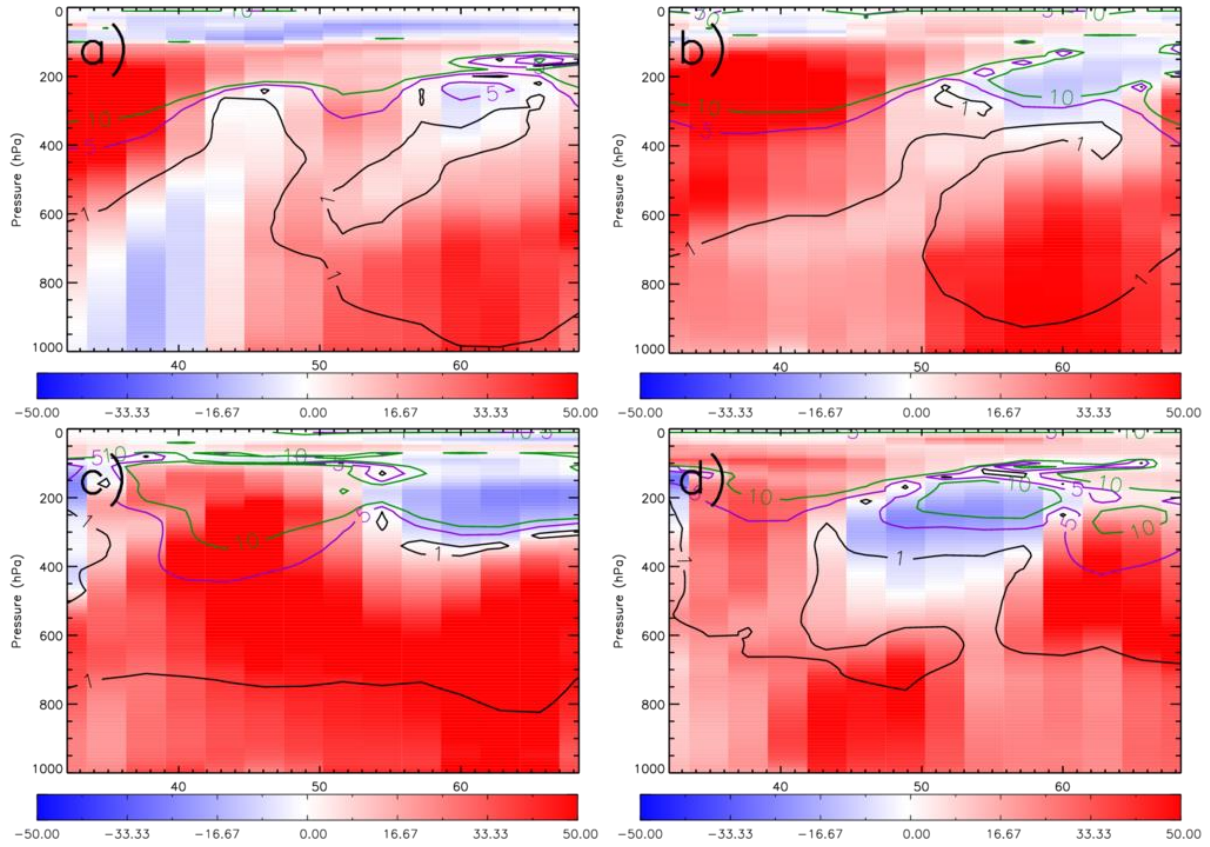
770



771

772 **Figure 9:** TOMCAT ozone, zonally averaged between 20°W and 40°E, 2018-2017 percentage  
 773 differences (absolute difference (ppbv) shown as solid lines) from the control simulation. Panels a)-d)  
 774 represent the monthly averages for May, June, July and August.

775



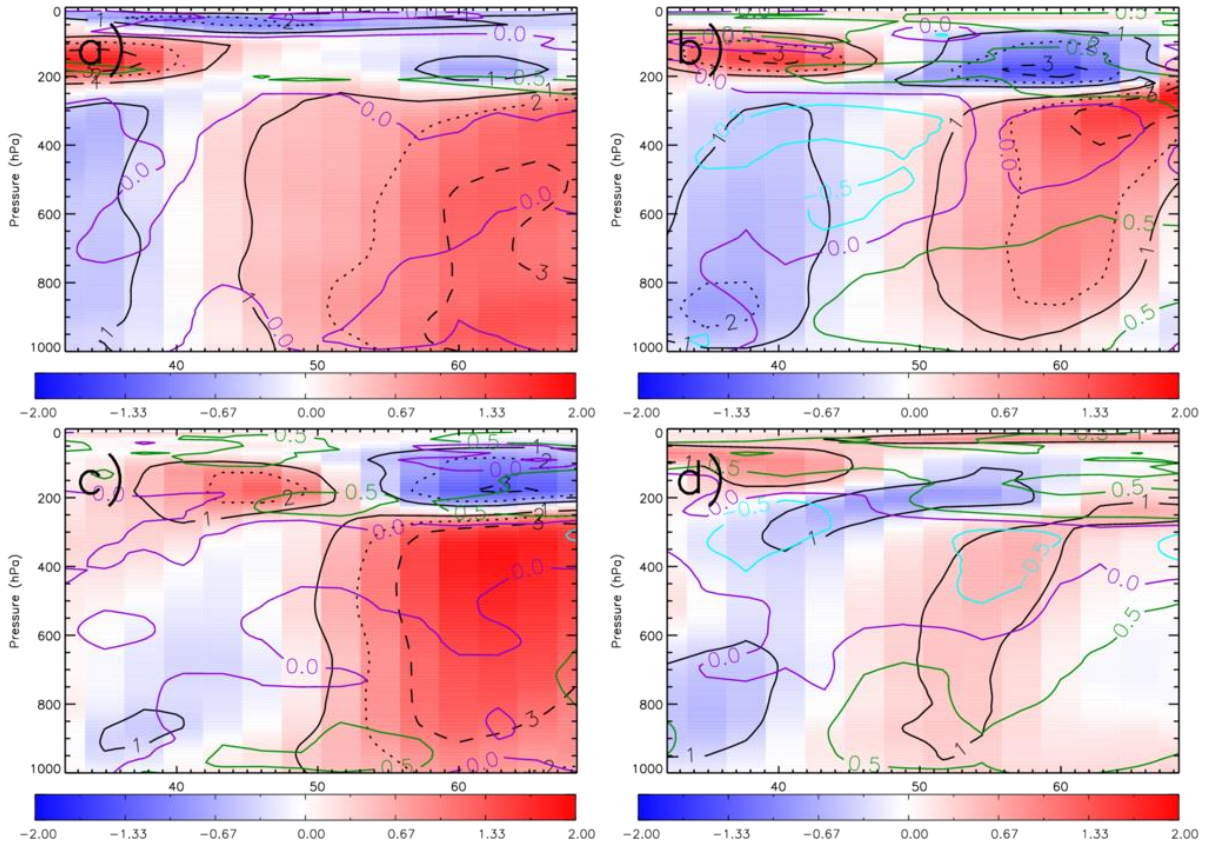
776

777 **Figure 10:** TOMCAT stratospheric ozone tracer, zonally averaged between 20°W and 40°E, 2018-2017  
 778 percentage differences (absolute difference (ppbv) shown as solid lines) from the control simulation.  
 779 Panels a)-d) represent the monthly averages for May, June, July and August.

780

781

782



783

784 **Figure 11:** TOMCAT temperature, zonally averaged between 20°W and 40°E, 2018-2017 percentage  
 785 differences (absolute difference (K) shown by black solid, dotted and dashed lines) from the control  
 786 simulation. Overplotted are contours of the temporal correlation (i.e. within each grid box) between  
 787 the temperature and ozone 2018-2017 differences. Panels a)-d) represent the monthly averages for  
 788 May, June, July and August.

789

790

791

792

793

794

795

796

797

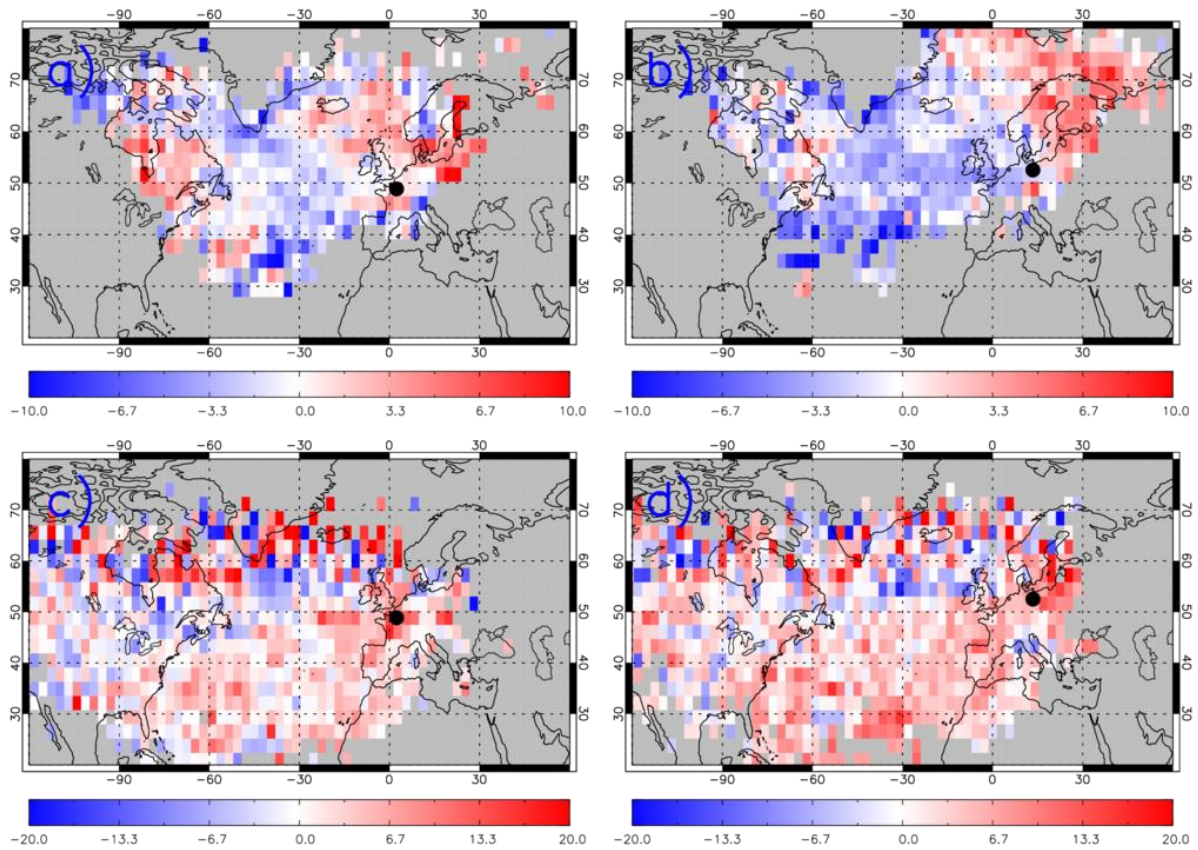
798

799

800

801

802



803

804

805

806

807

808

809

**Figure 12:** The difference between May-August 2018 and May-August 2017 (i.e. 2018-2017) ROTRAJ back-trajectories (10 days), weighted by the average TOMCAT  $O_3$  (ppbv) concentration along each trajectory path, gridded onto the TOMCAT horizontal resolution for a) Paris at the surface, b) Berlin at the surface, c) Paris at approximately 500 hPa and d) Berlin at approximately 500 hPa. The black circles represent the location of Paris or Berlin, where the trajectories were released from.